4
ENSO Diversity

Antonietta Capotondi[1,2], Andrew T. Wittenberg[3], Jong-Seong Kug[4], Ken Takahashi[5], and Michael J. McPhaden[6]

ABSTRACT

ENSO events display large interevent differences in amplitude, spatial pattern, and temporal evolution. The differences in spatial pattern, which have important consequences for ENSO teleconnections and societal impacts, have become known as "ENSO diversity." In this chapter we review key aspects of ENSO diversity, including ENSO's surface and subsurface characteristics, underlying dynamics, predictability, low-frequency variations, and long-term evolution, as well as the representation of ENSO diversity in climate models. To better understand the origin of ENSO diversity and identify specific characteristics of different event types, many different classification schemes have been proposed. Here we describe these different approaches and the insights they may provide on the nature of event-to-event differences. The last two decades have seen a greater number of El Niño events with the largest sea surface temperature anomalies in the central Pacific. Current research seeks to determine whether such changes in ENSO characteristics were the result of anthropogenic greenhouse gas forcing or just a manifestation of natural variability, and whether and how climate change may affect ENSO diversity in the future.

4.1. INTRODUCTION

The first El Niño of the 21st century in 2002–2003 was different than preceding El Niños, especially the 1997–1998 event (McPhaden, 2004). While the 1997–1998 El Niño achieved extreme sea surface temperature anomaly (SSTA) values in the eastern equatorial Pacific (Figure 4.1a), the largest SSTAs in the winter of 2002–2003 were weaker and primarily confined to the central equatorial Pacific (~170°W, Figure 4.1b). This event marked the start of a seemingly atypical ENSO evolution during the following decade, with relatively weaker and more frequent El Niño events, occurring approximately every two years, and whose largest SSTAs were in the central equatorial Pacific, albeit with differences in the detailed spatial pattern and evolution (e.g., the 2009–2010 event, Figure 4.1c). The 2000–2014 period culminated with the strong 2015–2016 El Niño event, which exhibited SSTAs comparable in magnitude to those of the 1997–1998 event, but displaced further west than in 1997–1998 (Figure 4.1d). A commonly reliable predictor of El Niño events, the equatorial Pacific upper-ocean warm water volume, became less useful as an ENSO precursor during 2000–2014, suggesting that some aspects of ENSO dynamics involving the evolution of the thermocline were different than in preceding decades (McPhaden, 2012; Luebbecke & McPhaden, 2014; Cai et al., 2018). In 2017, a "coastal El Niño" produced severe flooding in Peru, even though ENSO was neutral (Garreaud, 2018; Takahashi et al., 2018; Z.-Z. Hu et al., 2019; Peng et al.,

[1] *University of Colorado, CIRES, Boulder, CO, USA*
[2] *NOAA Physical Sciences Laboratory, Boulder, CO, USA*
[3] *NOAA Geophysical Fluid Dynamics Laboratory, Princeton, NJ, USA*
[4] *Division of Environmental Science & Engineering, Pohang University of Science and Technology (POSTECH), Pohang, Republic of Korea*
[5] *Servicio Nacional de Meteorología e Hidrología del Perú—SENAMHI, Lima, Peru*
[6] *NOAA Pacific Marine Environmental Laboratory, Seattle, WA, USA*

El Niño Southern Oscillation in a Changing Climate, Geophysical Monograph 253, First Edition.
Edited by Michael J. McPhaden, Agus Santoso, and Wenju Cai.

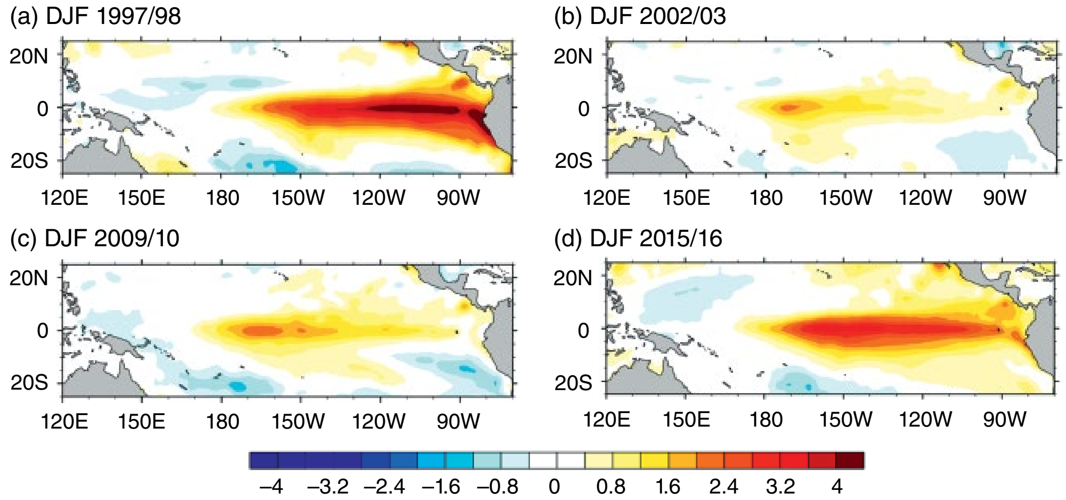

Figure 4.1 Interannual SST anomalies during December-January-February (DJF) for the El Niño events of (a) 1997–1998, (b) 2002–2003, (c) 2009–2010, and (d) 2015–2016. Monthly SST data were obtained from the NOAA Optimum Interpolation (OISST) data set (Reynolds et al., 2002). Anomalies are computed relative to the 1982–2017 climatology.

2019). This changing character of ENSO has stimulated a renewed interest in the nature of this powerful phenomenon, and in the fundamental causes of event-to-event differences. Research on ENSO diversity has primarily focused on the El Niño phase, since La Niña SSTAs tend to peak in the central Pacific with more limited longitudinal excursions (Kug & Ham, 2011), although subsurface characteristics can actually show greater diversity for La Niña than El Niño (Ashok et al., 2017).

While these event-to-event differences were initially described in terms of two different types, or "flavors," of El Niño, commonly referred to as eastern Pacific (EP) and central Pacific (CP) following the definition introduced by Kao and Yu (2009), it has become increasingly clear that El Niño events (and to a lesser degree, La Niña events) exhibit a wide spectrum of spatial structures. In particular, the location of maximum SSTAs along the equator spans a broad range of longitudes rather than clustering around only two locations (Giese & Ray, 2011), except perhaps for the extreme El Niño in the eastern Pacific (Takahashi et al., 2011, 2018). This wide range of spatial patterns, whose precise statistical distribution is somewhat clouded by observational uncertainties (Marathe et al., 2015), is illustrated by the longitudinal profiles of SSTAs along the equator for the El Niño events that occurred during 1951–2017 (Figure 4.2). Although these profiles may be broadly classified in two different groups, a large diversity of longitudinal structures can be seen among events. Indeed, to account for events that share elements of both EP and CP types, Kug et al. (2009) introduced a "mixed" El Niño type, with largest SSTAs in the Niño-3.4 region (5°S–5°N, 170°–120°W). El Niño events with SST anomalies that extended all the way to the eastern Pacific during some periods of their evolution, like the 2009 and 2014 CP events, were described as "basin-wide warming events" by Ashok et al. (2012) and Jadhav et al. (2015). It is evident from Figure 4.2 that CP events (blue-dashed lines) tend to be generally weak to moderate in strength, while events with the largest anomalies in the eastern equatorial Pacific exhibit a broader range of amplitudes from relatively weak to extreme (red dashed lines in Figure 4.2). An exception to the above description is the recent 2015–2016 El Niño, which achieved SSTAs typical of extreme events in the Niño-3.4 region (5°S–5°N, 120°–170°W) but exhibited only half of the amplitude seen in the previous extreme events in the far eastern Pacific (Figures 4.1d and 4.2; L'Heureux et al., 2017; Newman et al., 2018), so that the peak SSTA was located closer to the central Pacific.

Empirical dynamical models constructed from observed SSTs, thermocline depth, and zonal surface wind stress anomalies over the period 1959–2000 (Newman et al., 2011) indicate the presence of growing modes similar to EP and CP El Niño events. These results suggest that the broad range of observed El Niño types may arise from the superposition of these basic modes/structures, which themselves result from different dynamical balances, as mediated by the background conditions. Due to their differences in growth rate and dominant timescale, these two modes can give rise to complex ENSO behavior in both spatial and temporal domains (Timmerman et al., 2018).

In this chapter, we provide a synthesis of our current understanding of ENSO diversity. Section 4.2 reviews the

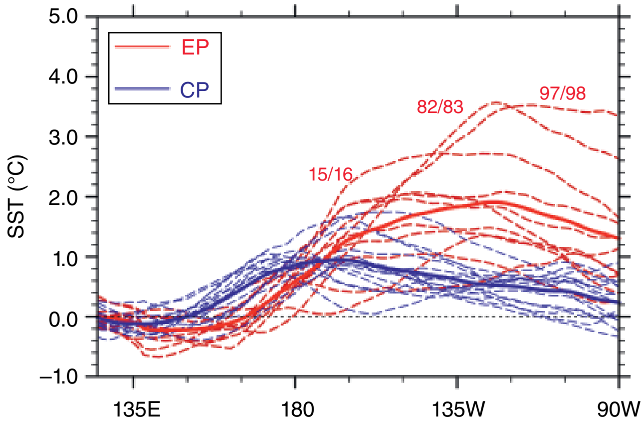

Figure 4.2 Equatorial SST anomaly profiles averaged over 2°S–2°N during winter (DJF) for CP (blue) and EP (red) El Niño events over the period January 1951–December 2017. The EP and CP events have been identified using the Niño-3 and Niño-4 indices: The DJF Niño-3 index is larger than 0.5°C and larger than the Niño-4 index for EP events, while the Niño-4 index is larger than 0.5°C and larger than the Niño-3 index for CP events. Thin dashed lines show the profiles of individual events, while the thick red and blue solid lines indicate the composite profiles for EP and CP El Niño events, respectively. Monthly SST data were obtained from the NOAA Extended Reconstructed SST dataset version 5 (ERSSTv5; Huang et al., 2017). Anomalies were computed relative to the 1951–2017 climatology, and linearly detrended prior to the profile calculation. The extreme events of 1982–1983, 1997–1998, and 2015–2016 are labeled.

large variety of approaches and indices proposed to capture the differences in El Niño spatial patterns, while section 4.3 describes the leading dynamical processes underlying different El Niño types. The precursors of these different El Niño types, and their influence on the predictability of ENSO diversity, are discussed in section 4.4; the low-frequency modulation and long-term trend of ENSO diversity are presented in section 4.5; and the ability of climate models to simulate ENSO diversity is discussed in section 4.6. Conclusions and future directions are presented in section 4.7.

4.2. CHARACTERISTICS OF ENSO DIVERSITY

It has long been recognized that "no two El Niño events are quite alike" (Wyrtki, 1975), but only in the early 2000s were these differences more systematically classified through the introduction of specific indices to characterize different types of El Niño events. The need for a more systematic classification has largely been motivated by the recognition that the details of ENSO spatial patterns may play an important role in ENSO teleconnections and societal impacts. Larkin and Harrison (2005), for instance, noticed that "conventional" El Niños (events with their largest SSTAs in the eastern Pacific) were associated with surface temperature and precipitation anomalies over the US that differed in spatial pattern, and in some locations even in sign, from those associated with "dateline" El Niños (events with their largest SSTAs in the central Pacific near the dateline). Although the statistical significance of the results was not very high due to the small sample size of the two classes of events, the possibility that El Niño spatial pattern could exert such an influence on quantities of large societal importance drew much attention to the diversity of ENSO events. Ashok et al. (2007) further emphasized the importance of the location of equatorial Pacific warming for atmospheric teleconnections, in particular those associated with the summer Indian monsoon as well as precipitation over Korea and Japan. Ashok et al. (2007) identified a specific pattern of SSTAs, characterized by positive anomalies in the central equatorial Pacific and cold anomalies in the eastern and western parts of the basin, which appeared responsible for those teleconnections, and which they called "El Niño Modoki," a Japanese word that means "similar but different" (see the appendix to this chapter for a definition of the El Niño Modoki index). Further discussion of the influence of ENSO diversity on teleconnections is provided in chapter 14.

The papers by Larkin and Harrison (2005) and Ashok et al. (2007) stimulated intense research activity on ENSO diversity (Capotondi et al., 2015a). To better characterize this diversity, it is useful to classify El Niño events into different categories to more easily identify differences in the leading dynamical processes, precursors, and impacts. To that end, several indices have been introduced to properly capture aspects of these El Niño groups, and different names have been suggested to define them. These names include, among others, Dateline El Niño and El Niño Modoki as mentioned above, and also warm pool (vs. cold tongue El Niño) and central Pacific (vs. eastern Pacific) El Niño. For simplicity, here we will refer to events with the largest SSTA in the eastern Pacific as "EP" and those with the largest SSTA in the central Pacific as "CP" El Niño types. A list of the most common indices introduced to classify these types is provided in the appendix.

Different definitions, and the exact details of their implementation, can lead to differences in the classification of individual events. For the NOAA-ERSSTv5 data set, Table 4.1 shows that some events can be either EP or CP depending on the indices used (e.g. 1965–1966 and 1991–1992), and the season chosen to define El Niño events can also play a role in the event classification. A dependency on the specific SST data set used can also be expected (Diamond & Bennartz, 2015).

Despite these discrepancies, similar average spatial characteristics of EP and CP events emerge with most of the proposed indices. Since the Niño-3 region (5°S–5°N, 90°–150°W) is located in the eastern Pacific, and the Niño-4 region (5°S–5°N, 160°E-150°W) in the central Pacific, the Niño-3 and Niño-4 indices (SSTAs averaged over the Niño-3 and Niño-4 regions, respectively) have been widely used to identify EP and CP El Niño events (Kug et al., 2009; Yeh et al., 2009; Kug et al., 2010; Capotondi, 2013; see the appendix for definitions). Composites of the EP and CP events obtained with this approach (Figure 4.3) show that EP events have SSTAs that peak further east, as expected, but are also, on average, stronger than CP events. Sea surface height (SSH) anomalies, which are dynamically linked to thermocline depth, show a strong zonal dipole in the case of EP events (Figure 4.3, top left), indicative of a deeper thermocline in the eastern and shallower thermocline in the western equatorial Pacific. CP events (Figure 4.3, top right), on the other hand, are characterized by weaker positive thermocline depth anomalies that extend further westward than for EP events, and negative thermocline depth anomalies confined to the far western Pacific. Sea level pressure (SLP) anomalies (Figure 4.3, middle panels) in the tropical Pacific exhibit the zonal seesaw typical of the Southern Oscillation (SO), with higher than average pressure in the western part of the basin and lower than average pressure in the eastern tropical Pacific. These

Table 4.1 Classification of El Niño events based on some of the commonly used indices described in the appendix. These indices include the Niño-3/Niño-4 approach, using either 0.5°C or one standard deviation as thresholds for event identification (first two columns); the E and C indices of Takahashi et al. (2011, column 3); the Modoki index (EMI, Ashok et al., 2007) to identify CP-Modoki events (column 4), and the EP_{new} and CP_{new} indices of Sullivan et al. (2016). Notice that for the EMI we do not apply the criterion that the anomalous warming in the central Pacific must persist from boreal summer through winter as in Ashok et al. (2007). When this criterion is applied, the 2009–2010 El Niño does not qualify as an El Niño Modoki. Monthly SSTs from the NOAA-ERSSTv5 data set over the period 1951–2017 have been used to prepare the table. EP events (denoted with "E") are highlighted in red, while CP events (denoted with "C") are shown in green. Since different winter seasons have been used in the literature to select El Niño events, we have considered both the November-December-January (NDJ), and the December-January-February (DJF) seasons. In those cases when results differ in the two seasons, subscripts are used to indicate the season. Notice that in some cases events start as EP events in NDJ and evolve into CP events in DJF, or vice versa, as indicated by the arrow. The blank entries indicate cases in which the SSTA conditions were not detected as an El Niño with those indices. In the "Consensus" column, an El Niño is registered as a consensus event if it gets at least two votes from among the five different methods. It is then labeled as E or C if it has a margin of at least two votes in favor of either E or C, respectively, while a "no consensus" case is indicated by a question mark.

	Niño-3/Niño-4 > 0.5°C	Niño-3/Niño-4 > 1 std	E/C	Modoki	EP_{new}/CP_{new}	Consensus
1951–1952	E		E_{NDJ}		E_{NDJ}	**E**
1953–1954	C					
1957–1958	E	E	C		E	**E**
1958–1959	C_{NDJ}			C	C_{NDJ}	**C**
1963–1964	E		C_{NDJ}			**?**
1965–1966	E	E	C	C	E	**?**
1968–1969	C	C	C	C	C	**C**
1969–1970	$E_{NDJ} \rightarrow C_{DJF}$					
1972–1973	E	E	E		E	**E**
1976–1977	E				E	**E**
1977–1978	C			C	C	**C**
1979–1980	$E_{NDJ} \rightarrow C_{DJF}$					
1982–1983	E	E	E		E	**E**
1986–1987	E	E_{DJF}	$C_{NDJ} \rightarrow E_{DJF}$		E	**E**
1987–1988	$E_{NDJ} \rightarrow C_{DJF}$	C	C		C	**C**
1991–1992	E	E	C	C	E	**?**
1994–1995	C	C	C	C	C	**C**
1997–1998	E	E	E		E	**E**
2002–2003	$E_{NDJ} \rightarrow C_{DJF}$	C_{NDJ}	C	C_{DJF}	C	**C**
2004–2005	C	C	C	C	C	**C**
2006–2007	$E_{NDJ} \rightarrow C_{DJF}$	C_{NDJ}	C_{NDJ}		C	**C**
2009–2010	C	C	C	C	C	**C**
2014–2015	C			C_{DJF}	C	**C**
2015–2016	E	E	$E_{NDJ} \rightarrow C_{DJF}$		E	**E**

SLP anomalies are associated with westerly wind anomalies along the equator, which are part of the positive feedback known as the Bjerknes feedback, that promotes El Niño anomaly growth. While EP events (Figure 4.3c) exhibit strong westerly wind anomalies extending to ~120°W, with northerly wind anomalies further east, CP events (Figure 4.3d) have a weaker equatorial SLP gradient that is located further to the west, so that the associated westerly wind anomalies are weaker and confined westward of ~150°W, while southeasterly wind anomalies are seen in the eastern part of the basin (Harrison & Chiodi, 2009). Similarly, precipitation anomalies (Figure 4.3, bottom panels) extend all the way to the South American coast in the case of EP events, while they are limited to the western part of the basin during CP events. In the extratropical North Pacific, El Niño events are associated with a deepened and eastward-extended Aleutian Low, and with a deeper thermocline and warmer conditions along the West Coast of North America. Positive anomalies of SST and SSH are also seen along the coast of South America. These El Niño influences, which are critical for marine ecosystem dynamics along the west coasts of the Americas, appear to be more pronounced during EP events.

Although useful for classifying ENSO events, the Niño-3 and Niño-4 indices are highly correlated with each other (the correlation coefficient for the indices used to produce Figure 4.3 is 0.84), so that they are not suitable indices for describing the distinctive evolution of EP and CP events. Other indices that are largely uncorrelated with each other have therefore been introduced. For example, the EP_{new} and CP_{new} indices (see the appendix for definition) proposed by Sullivan et al. (2016) have been used to highlight the differences in skewness and spectral characteristics of the EP and CP events, as illustrated in Figure 4.4 for the time period 1951–2017. While the EP_{new} index has a positive skewness (warm events tend to be larger than cold events; Figure 4.4a) and has spectral peaks at about 1.2 and 3–5 years (Figure 4.4b), the CP_{new} index displays a negative skewness (negative events tend to be larger than positive events, Figure 4.4c) with enhanced spectral power around 2–2.5 years and in the decadal range (Figure 4.4d). CP activity with a quasi-biennial timescale appears, indeed, to undergo a quasi-decadal modulation, with multiyear periods dominated by CP La Niñas followed by multiyear periods populated with CP El Niños, as highlighted by the seven-year low-pass filtered time series in Figure 4.4c. The predominance of CP events in the early 21st century, as seen in Figure 4.4c, had an imprint on the equatorial sea level, which was above average in the central Pacific and below average near the eastern and western boundaries during 2000–2004 (Behera & Yamagata, 2010). Differences in skewness and spectral characteristics were also noticed by Yu et al. (2011) using the subsurface EP and CP indices (see appendix), but no decadal variability was identified with those indices.

As stressed by Trenberth and Stepaniak (2001), two indices are needed to characterize differences in spatial patterns and temporal evolution of El Niño events. Since ENSO-related equatorial SST variability has low dimensionality (Karamperidou et al. 2014), the two leading empirical orthogonal functions (EOFs) of SSTA can jointly explain a large fraction of the variance of typical ENSO SST indices (Takahashi et al., 2011). The leading EOF of equatorial SSTAs resembles a canonical El Niño pattern, with the largest anomalies in the Niño-3.4 region and the same sign in the central and eastern equatorial Pacific, while the second EOF exhibits differences in sign between the eastern and central Pacific. Thus, the linear combination of these two EOFs, as described in the appendix, produces patterns characterized by enhanced warming in the far eastern (E pattern) or central (C pattern) equatorial Pacific, as seen in Figures 4.6a and 4.6b, respectively. Similar patterns can be obtained by considering alternative quasi-orthogonal indices, like the Niño-3 index and the Trans-Niño index (TNI; Trenberth & Stepaniak, 2001; see appendix for definition) as descriptors of ENSO diversity. The spatial pattern associated with the TNI displays a zonal SST dipole in the equatorial region, similar to that of the second EOF of SST, so that a linear combination of the Niño-3 and TNI indices results in patterns that are very similar to the E and C patterns (Santoso et al., 2017). The relationship between various indices of ENSO diversity in the space of the two leading principal components (PCs, the projection of the SSTA on the two leading EOF patterns at each time step) is shown in Figure 4.5. Because most of the SSTA variance lies near the PC1/PC2 plane, the linear correlation between any two indices is approximately given by the cosine of the angle between their corresponding axes in Figure 4.5. Thus, orthogonal axes indicate maximum independence between two indices, as is the case of the E and C indices, which are derived from the first two EOF modes and represent SST variability that can be exclusively attributed to the eastern and central equatorial Pacific, respectively (Takahashi et al., 2011). The extreme El Niño events of 1877–1878, 1982–1983, and 1997–1998 had much higher values of E (as well as Niño-1+2 and EP_{new}) than any other year, and it has been suggested that these events belong to a distinct dynamical regime (Takahashi et al., 2011; Takahashi & Dewitte, 2016). Thus, El Niño amplitude diversity (strong vs. moderate/weak) is an important aspect to consider.

El Niño events also differ in their temporal evolution. Using lag-correlation analysis, Kao and Yu (2009) showed that EP El Niño SSTAs tend to develop in the eastern equatorial Pacific and propagate westward, as in

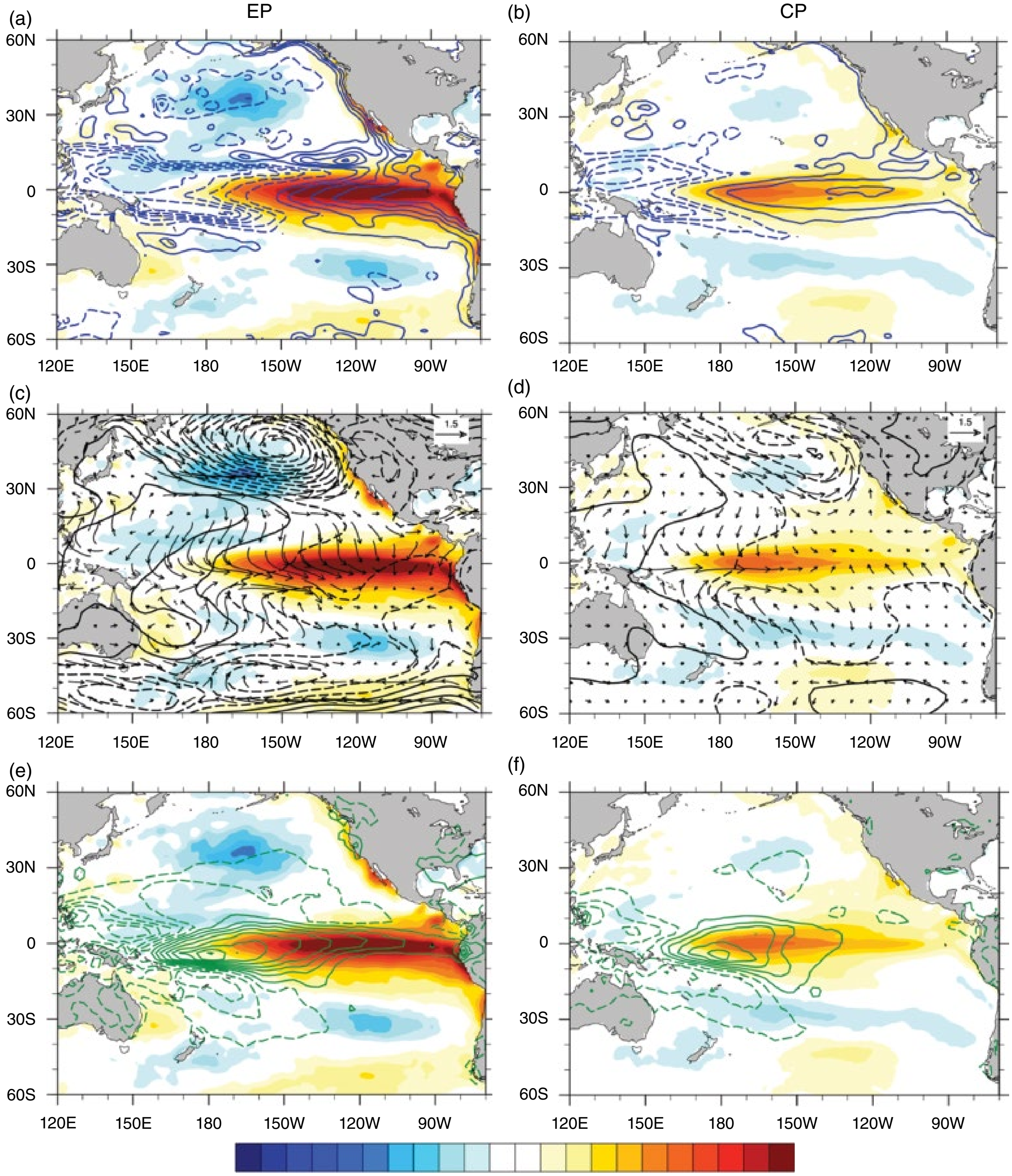

Figure 4.3 Composites of anomalous SST (shaded, °C, same in each row), SSH (top, contours), SLP/Winds (middle, contours/vectors), and Precipitation (bottom, contours) for EP (left), and CP (right) El Niño events during winter (DJF). Contour intervals are 2 cm for SSH, 0.7 millibars for SLP, and 0.7 mm/day for precipitation. Vector winds are in m/s. Dashed contours indicate negative values. The EP and CP events have been identified using the Niño-3–Niño-4 index approach (appendix). Events are considered EP when the DJF Niño-3 index is larger than the DJF Niño-4 index, and larger than 0.5°C, while CP events are characterized by the DJF Niño-4 index being larger than the DJF Niño-3 index, and larger than 0.5°C. The SST and SSH fields are obtained from the ECMWF ORAS4 ocean reanalysis (Balmaseda et al., 2013) over the period January 1958–December 2015, SLP and surface winds are from the NCEP-NCAR reanalysis (Kalney et al., 1996), while precipitation is obtained from a reconstructed data set over the global land and ocean (Chen et al., 2002). Anomalies are relative to the 1958–2015 climatology. All fields have been linearly detrended prior to the composite calculation.

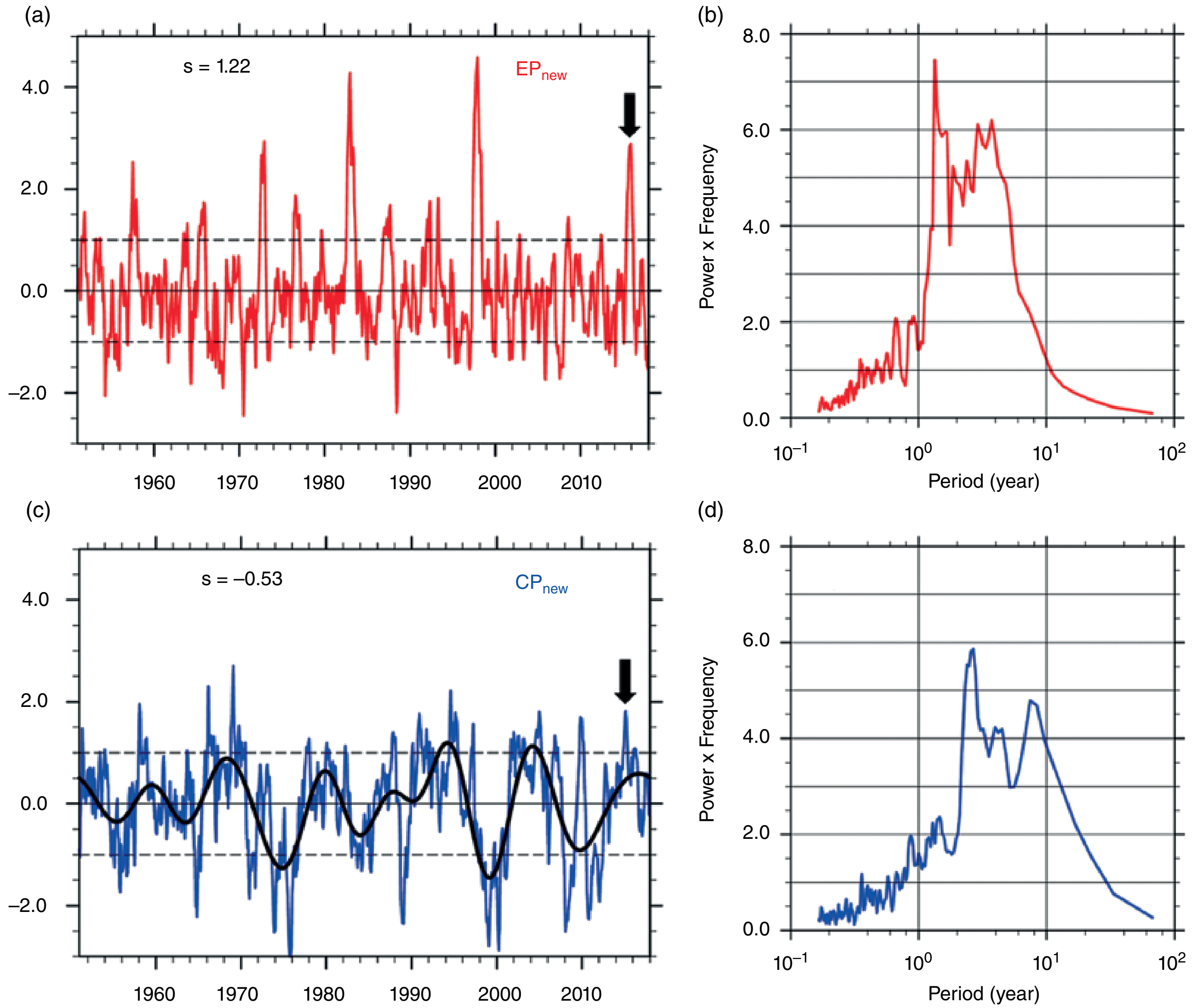

Figure 4.4 (a) and (c) show the time series of the EP_{new} and CP_{new} indices, as defined by Sullivan et al. (2016), while (b) and (d) show the corresponding spectra in variance preserving form. Both time series are normalized to unit standard deviation. Notice that both indices are above one standard deviation (dashed line) during the 2015–2016 El Niño event (black arrow in a and c), consistent with the classification of this event as a mixture of CP and EP types (Paek et al., 2017). The CP_{new} index has a spectral peak close to 10 years; this quasi-decadal component is evident in the 7-year low-pass filtered time series (thick black line in c). The s-values indicate skewness. Monthly SST data are from the ERSSTv5 dataset over the period 1951–2017.

the case of the "canonical El Niño" described by Rasmusson and Carpenter (1982), while CP events develop in the central Pacific near the dateline without a clear zonal propagation direction (Xiang et al., 2013). These central equatorial Pacific anomalies are often the equatorial signature of SSTAs that extend from the U.S. West Coast near Baja California toward the equator, associated with the Pacific meridional mode (Chiang & Vimont, 2004), as further discussed in section 4.4. The statistical description of the EP event propagation outlined by Kao and Yu (2009) has some notable exceptions, like the extreme El Niño events of 1982–1983 and 1997–1998. SSTAs during 1982 events developed in the central Pacific and propagated eastward, while during 1997 SSTAs above 1°C appeared simultaneously in the western and eastern Pacific during February and merged in the central Pacific. In contrast to the east or west direction of SSTA propagation along the equator during El Niño events, SSTAs during La Niña events generally propagate only to the west (McPhaden & Zhang, 2009).

Another approach to identify "flavors" of spatiotemporal diversity makes use of EOF analysis of the

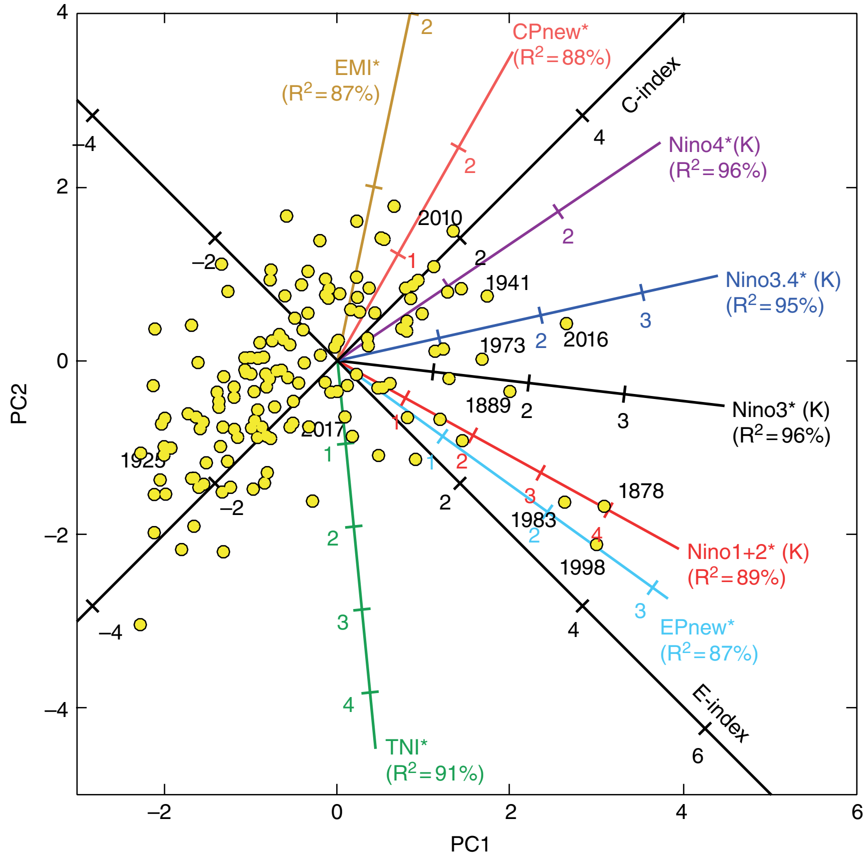

Figure 4.5 December–February (DJF) mean equatorial Pacific (10°S–10°N) SSTA PC1 and PC2 from ERSSTv5 (1870–2018, climatology based on 1981–2010) following Takahashi et al. (2011). Values of various ENSO indices estimated with multiple linear regression with these PCs can be obtained by reading the values from the corresponding axes (variance explained for 1950–2017 indicated as R^2).

longitudinal and temporal evolution of the SSTA fields along the equator between 5°S and 5°N (see appendix; Lee et al., 2014; Dewitte & Takahashi, 2019). In addition to capturing the diversity of amplitude and spatial pattern, this method also captures the large interevent diversity of SSTA evolution following the event peak, for example, distinguishing El Niños that persist through boreal spring from more short-lived El Niños, and distinguishing resurgent El Niños from those that transition into La Niñas. These temporal details of ENSO evolution are critical for ENSO's remote impacts, since many of the teleconnections and local conditions are strongly affected by the seasonal cycle. For example, Lee et al. (2016) found that El Niños that persist into boreal spring (such as the 2015–2016 event) are associated with reduced risk of tornado outbreaks over most of the U.S., while early-terminating El Niños boost the likelihood of tornado outbreaks in the upper Midwest by up to 50% in May. Similarly, strong La Niñas that persist through boreal spring (such as the 1974 and 2011 events) enhance the likelihood of tornado outbreaks over the Ohio Valley, Southeast U.S., and upper Midwest in boreal spring, while La Niñas that transition to El Niños boost the likelihood of outbreaks in the southern U.S. In another study, Lee et al. (2018) showed that only strong El Niños that persisted into boreal spring (like the 1982 and 1997 events) were associated with increased rainfall over the entire state of California, while transitioning El Niños enhanced rainfall mainly over northern California, and weak El Niños showed little impact on California rainfall.

A characterization of ENSO diversity from an ocean energetics perspective is provided by the perturbation available potential energy (APE; Goddard & Philander, 2000; Brown & Fedorov, 2010; Hu et al., 2014), a quantity that measures the energy potentially available to the system from a horizontal redistribution of mass, as a result of the work done by the winds on the ocean. A positive APA corresponds to a steeper than average thermocline along the equator, and vice versa. A strong linear

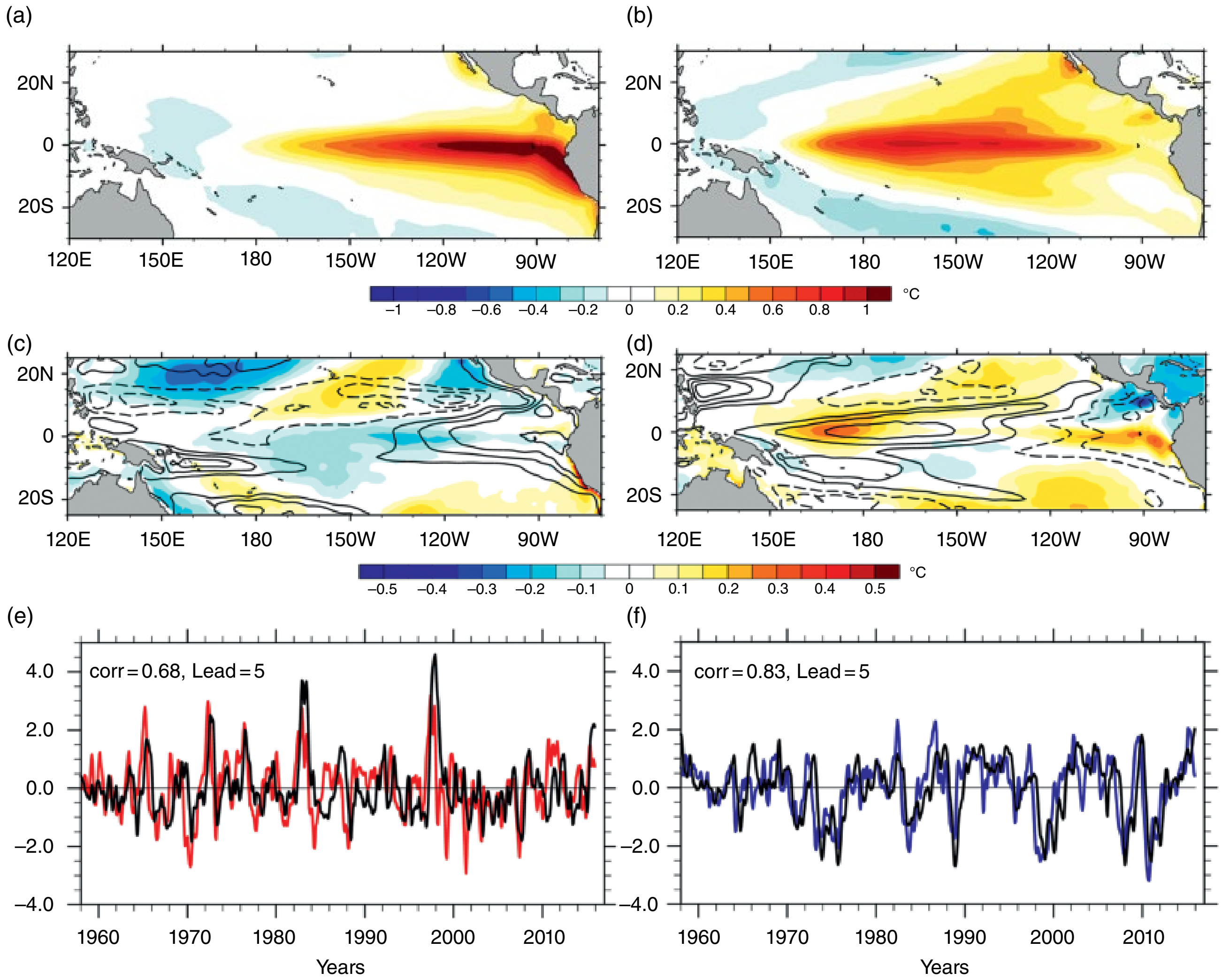

Figure 4.6 Optimal two-season precursors (c and d) of the (a) E and (b) C modes of Takahashi et al. (2011). See appendix for definition. The optimal precursors are computed as the tropical SST (shaded) and SSH (contoured) conditions that lead to the largest growth of the E and C indices six months later. If y is either the E or C index, and $\boldsymbol{x}$ the tropical state vector, as characterized by the 20 leading SST and 10 leading SSH EOFs, the optimal precursor $\boldsymbol{x}_{opt}$ can be obtained as the leading right singular vector of the operator $\boldsymbol{H}$, such that $y(t + \tau) = \boldsymbol{H}\,\boldsymbol{x}(t)$, where $\boldsymbol{H}$ is computed through multiple linear regressions. The time series of the optimal precursors for the E and C modes, computed as the projection of the SST and SSH fields onto the optimal structures at each time step (black lines), are compared in (e) and (f) with the E (red line) and C (blue line) indices, respectively. The largest correlations between the two sets of standardized indices (0.68 for the E index, and 0.83 for the C index) are obtained when the "optimal" indices lead the E and C indices by five to six months. SST and SSH data are from the ECMWF ORAS4 reanalysis during 1958–2015 (Balmaseda et al., 2013).

anticorrelation is found between APA and the Niño-3/Niño-4 ratio for all the El Niño events, with both Niño-3 and Niño-4 positive and either index greater than 0.5, indicating a preference for EP events to occur when the zonal slope of the thermocline is reduced relative to CP events (Hu et al., 2014).

Indices of ENSO diversity based on outgoing longwave radiation (OLR) have been introduced to more directly relate ENSO diversity to remote impacts (Chiodi & Harrison, 2010; Johnson & Kosaka, 2016; Williams & Patricola, 2018). OLR anomalies are an indication of atmospheric deep convection, which is a source of atmospheric teleconnections through the excitation of atmospheric Rossby waves. As the atmospheric Rossby waves propagate from the tropics to high latitudes, they alter the extratropical atmospheric circulation and its influence on surface air temperature and precipitation. A motivation for using OLR-based ENSO diversity indices is that deep convection in the eastern tropical Pacific tends to be associated with more robust impacts over the U.S. During EP El Niño events, in particular, the eastern Pacific SSTs may exceed the convective threshold (about 27.5°C; Graham & Barnett, 1987; Takahashi & Dewitte, 2016), so that convection can shift eastward and affect atmospheric teleconnections. Indeed, Figure 4.3 shows that precipitation, which is an indicator of deep convection, generally extends to the eastern tropical Pacific during EP events. Because of the relatively short OLR record dating back to 1979, however, the teleconnections associated with the eastern Pacific OLR signature are still relatively uncertain.

The EP and CP events that are identified by the various indices listed in the appendix have SSTAs that extend over a large portion of the equatorial Pacific. A different class of El Niño events includes cases in which high positive SSTAs develop rapidly along the coast of South America in the far eastern equatorial Pacific in boreal winter and spring, while the rest of the equatorial Pacific remains cold or neutral. Such events, called "coastal El Niños" (Takahashi & Martinez, 2019) can have devastating impacts on flooding in western South American countries, and are associated with a strengthening of the Intertropical Convergence Zone (ITCZ) south of the equator, and northerly wind anomalies across the equator in the far eastern Pacific. Notable examples were observed in 1891, 1925 (Schott, 1931; Takahashi & Martinez, 2018), and more recently in the boreal spring of 2017, a period characterized by torrential rains over the northern coastal areas of Peru, causing enormous losses of life and property (Fraser, 2017; Garreaud, 2018; Hu et al., 2019; Takahashi et al., 2018; Peng et al., 2019).

4.3. EQUATORIAL DYNAMICAL PROCESSES UNDERLYING ENSO DIVERSITY

One important question concerning ENSO diversity is whether EP- and CP-type events are governed by similar or different dynamical processes. Heat budget analysis has been used to identify the leading dynamical feedbacks responsible for the growth and decay of EP and CP events. The upper-ocean heat budget is computed at each grid point as the balance between the heat storage term, the oceanic advective terms (Q_{adv}), and the surface heat flux terms (Q_F) in a layer of depth H, usually chosen as the mean mixed layer, so that its temperature is approximately vertically homogeneous:

$$\rho c_p H \frac{\partial T}{\partial t} = Q_{adv} + Q_F + R, \tag{4.1}$$

where ρ is the density of seawater, c_p is the oceanic heat capacity, T is the upper-ocean temperature, t is time, and R is a residual term that accounts for omitted processes (e.g. vertical and lateral mixing, solar penetration, sub-monthly advection). Q_{adv} includes zonal, meridional, and vertical advection. For example, the vertical (Q_z) and zonal (Q_x) advection terms can be written as

$$Q_z = \rho c_p \int_{-H}^{0} -w \frac{\partial T}{\partial z} dz \text{ and } Q_x = \rho c_p \int_{-H}^{0} -u \frac{\partial T}{\partial x} dz,$$

where w and u are the vertical and zonal velocities, respectively, and z and x are the vertical and zonal coordinates. These terms can be further divided into linear and nonlinear components by separating each variable into its time mean and anomaly. Previous studies have recognized the leading role of two linear feedback terms:

$$\text{Thermocline feedback} = -\bar{w} \frac{\partial T'}{\partial z} \tag{4.2}$$

$$\text{Zonal advective feedback} = -u' \frac{\partial \bar{T}}{\partial x} \tag{4.3}$$

where the primes indicate anomalies and overbars denote climatological values. The thermocline feedback is the advection due to mean upwelling acting on the anomalous vertical temperature gradient, while the zonal advective feedback is the advection due to anomalous zonal currents acting on the mean zonal temperature gradient.

The relative importance of these feedbacks varies along the equator, because the oceanic and atmospheric background mean states are zonally asymmetric. In the eastern Pacific where the thermocline is shallow and upwelling is strong, anomalous thermocline variations play a large role in the SST tendency and lead to a strong thermocline feedback. In the central Pacific a deep mean thermocline suppresses the thermocline feedback, but the strong mean zonal temperature gradient at the warm pool edge, and strong zonal velocity anomalies induced by El Niño-related westerly wind anomalies, make SSTA growth sensitive to the zonal advective feedback. The longitudinal distribution of wind speed anomalies can also contribute to the spatial structure of CP events. CP El Niño westerly wind anomalies over the Niño-4 region reduce the local wind speed, which amplifies warm Niño-4 SSTAs due to reduced evaporation and vertical mixing; but increased easterlies in the eastern Pacific (Figure 4.3d) act to damp SSTAs in the Niño-3 region and contribute to the confinement of the SSTAs to the central Pacific (Kug et al., 2009).

Thus, the growth and decay of events centered at different longitudes can be expected to be controlled by different feedbacks. This is confirmed by a heat budget analysis of events peaking in different regions along the equator (Capotondi, 2013), which showed how the relative importance of the different feedbacks for the growth and decay of the events gradually varies along the equator, with the thermocline feedback dominating in the east and the zonal advective feedback becoming more important in the central Pacific. For this reason, EP events have been associated with the thermocline feedback and CP events with the zonal advective feedback. However, each El Niño event has a zonally broad structure that may extend beyond the eastern or central Pacific regions and be influenced by other processes. For instance, the warm anomalies of EP events that extend into the central Pacific (as seen for example during 1997–1998 in Figure 4.1a) can also see large contributions from zonal advection processes. Similarly, CP events with SSTAs in the eastern Pacific can see contributions from the thermocline feedback in that region.

The unique evolution of events with extreme eastern Pacific warming, like the 1877–1878, 1982–1983, and 1997–1998 events, distinguishes those events from moderate and CP El Niños (Figure 4.5). This difference has been explained in terms of the existence of an SST threshold (at about 27.5°C in the present-day climate) above which atmospheric deep convection can occur (Graham & Barnett, 1987). This threshold introduces a nonlinearity in the Bjerknes feedback that is particularly relevant in the eastern Pacific, where it would only be activated during extreme El Niños (Takahashi & Dewitte, 2016). Adding such nonlinearity to the damped recharge-discharge oscillator model, while keeping the system in a stable regime, is sufficient to generate bimodality associated with strong and moderate El Niños, although the action of high-frequency stochastic forcing blurs the mode separation in this model (Takahashi et al., 2019).

4.4. PRECURSORS AND PREDICTABILITY OF ENSO DIVERSITY

ENSO is often described as a low-frequency tropical mode of coupled ocean-atmosphere variability energized by stochastic wind forcing (Penland & Sardeshmukh, 1995). The "quasi-oscillatory" nature of ENSO, which alternates between warm and cold events approximately every two to seven years as measured by the equatorial SSTA, is connected with the evolution of the upper-ocean warm water volume (WWV) which undergoes meridional displacements toward and away from the equator, as described by the recharge oscillator paradigm for ENSO (Jin, 1997). The WWV, usually diagnosed as the volume of water above the thermocline between 5°S and 5°N and across the Pacific basin, has been a very useful precursor for ENSO events, with a "recharged" equatorial state (larger WWV) usually preceding the peak SSTAs in the Niño-3.4 region by about two to three seasons (Meinen & McPhaden, 2000). However, the relationship between WWV and ENSO SSTAs changed in the first decade of the 21st century, when WWV anomalies weakened and typically led the ENSO SSTAs only by one season (McPhaden, 2012). This changed relationship is likely associated with the dominance of CP El Niño events during that period. Indeed, the difference in the thermocline depth anomalies for EP and CP events, as seen in Figure 4.3 (top) is indicative of a different anomalous zonal thermocline tilt, and hence different anomalous meridional geostrophic flow, implying different recharge/discharge processes during the two event types. The large changes in the zonal slope of the thermocline during EP events lead to a rapid discharge of warm water from the equatorial thermocline, and a robust transition to a La Niña event immediately after the event peak. On the other hand, the smaller thermocline depth anomalies during CP events are associated with a much weaker discharge, a longer duration of the positive SSTAs, and a reduced likelihood of transitioning into a La Niña (Kug et al., 2009, Kug et al., 2010, Capotondi, 2013).

In addition to the oceanic thermocline processes, fast variations of the surface wind stress in the western and central equatorial Pacific also provide an important forcing mechanism for El Niño events. These fast wind stress variations, commonly referred to as westerly wind bursts (WWBs), excite downwelling oceanic Kelvin waves which can propagate all the way to the eastern part of the basin (McPhaden, 1999), where they deepen the thermocline and potentially initiate an El Niño event. The WWBs are often, but not always (Chiodi et al., 2014), associated with the Madden Julian Oscillation (MJO; Puy et al., 2016), as well as with tropical cyclones (Tian et al., 2018). The WWBs are considered to be a state-dependent stochastic wind forcing of ENSO as their frequency and intensity increase with warmer SST conditions (Lengaigne et al., 2004; Yu et al., 2003; Gebbie et al., 2007; Kug et al., 2008; Capotondi et al., 2018, and references therein). The interplay between the ocean subsurface conditions and WWB activity can contribute to diversity in both amplitude and spatial pattern, as shown by recent modeling studies (Hu et al., 2014; Fedorov et al., 2015; Jadhav et al., 2015; Levine et al., 2016; Puy et al., 2019). In particular, based on coupled model experiments, a subsurface "recharged" state would evolve into a moderate CP El Niño in the absence of WWBs but may develop into a strong EP El Niño in the presence of WWBs (Vecchi et al., 2006b). Similarly, a "discharged" state that would develop into a La Niña without WWB activity may result in a CP El Niño if WWBs are present. Seasonally, WWBs and related intraseasonal wind forcing in boreal spring are particularly effective at triggering El Niño events (McPhaden et al., 2006; Hendon et al., 2007; Lopez & Kirtman, 2014); in addition, the presence of westerly wind stress anomalies above a threshold in the central Pacific starting in August during the El Niño onset indicates an increased likelihood that the event will become an extreme El Niño (Takahashi & Dewitte, 2016).

Influences from regions outside the tropical Pacific have also been proposed as possible triggers of ENSO events and contributors to ENSO diversity. Within the Pacific basin, extratropical precursors include the Pacific meridional mode (PMM; Chiang & Vimont, 2004) in the Northern Hemisphere, and the south Pacific meridional mode (SPMM; Zhang et al., 2014) in the Southern Hemisphere. The equatorial SSTAs associated with the PMM occur in the central Pacific, so that the PMM has been viewed as a precursor for CP El Niño events (Yu and Kim, 2011; Vimont et al., 2014). The SPMM, on the other hand, is a mode of variability characterized by SSTAs in the southeastern tropical Pacific, and has been considered a possible precursor for EP events (Zhang et al., 2014; Vimont et al., 2014). Modulation of the trade winds by the southern lobe of the North Pacific Oscillation (Rogers, 1981; Linkin & Nigam, 2008), the second leading mode of wintertime SLP variability over the north Pacific, produces subtropical SSTAs that can propagate southwestward via a wind-evaporation-SST feedback (Xie, 1999) and promote the development of an ENSO event after they reach the equator (Chang et al., 2007). Wind stress curl anomalies associated with the PMM can also force an equatorward meridional transport which alters the equatorial heat content and favors the development of El Niño events, a mechanism known as "trade wind charging" (TWC; Anderson & Perez, 2015).

Apart from the SST precursors, the subsurface initial state of the ocean appears to be a critical discriminating factor in the development of an EP or CP event (Capotondi & Sardeshmukh, 2015). Here we apply the same methodology of Capotondi & Sardeshmukh (2015) to time series of tropical SST and SSH anomalies from the ECMWF ORAS4 ocean reanalysis (Balmaseda et al., 2013), to determine the optimal precursors for EP and CP events at a 6-month lead time. The latter are identified using the E and C indices of Takahashi et al. (2011). The E and C spatial patterns, computed as the regression of SSTAs on the E and C indices (Takahashi et al., 2011), are shown in Figures 4.6 a and b, respectively. The 20 leading EOFs of SST and 10 leading EOFs of SSH anomalies between 25°S and 25°N are used to characterize the state of the equatorial ocean. The optimal SST and SSH initial conditions for the EP and CP events are shown in Figures 4.6 c and d, respectively. Both initial conditions exhibit similar positive SST structures that are reminiscent of the PMM, SPMM, and northwest Pacific precursor (cold SSTAs in the northwestern tropical Pacific; Wang et al., 2012), although with different relative strengths in the two cases. However, the SSH fields show positive anomalies (deeper thermocline) in the eastern equatorial Pacific, extending westward to the dateline for EP events, but negative anomalies (shallower thermocline) in the eastern Pacific in the case of CP events, in agreement with the results of Capotondi & Sardeshmukh (2015). The indices associated with the two optimal initial conditions, obtained by projecting the SST and SSH fields at each time step on the optimal patterns, are largely correlated with the E and C indices at a six-month lead time (0.71 for EP, and 0.84 for CP, Figures 4.6 e and f). Given the critical role played by the zonal thermocline slope on event selection, it is conceivable that La Niña–like background conditions (similar to those present during the first decade of the 21st century) may be more conducive to the development of CP events.

Influences from other ocean basins may also contribute to ENSO diversity. North Tropical Atlantic (NTA) SST variations in boreal spring appear to favor the development of ENSO events by creating strong air-sea interactions along the Pacific ITCZ (Ham & Kug, 2013a). In particular, NTA cooling is more conducive to the occurrence of CP El Niño events. In contrast to the NTA SSTAs, the Atlantic Niño in boreal summer is more related to the development of EP El Niño events (Ham et al., 2013b). These studies thus suggest that these two tropical Atlantic precursors may contribute to ENSO diversity to some extent, so that prediction of ENSO diversity in dynamical models may potentially be improved if the models simulate tropical Atlantic variability realistically.

How predictable are EP and CP El Niño events? While the SST and SSH precursors in Figure 4.6 indicate some degree of predictability for EP and CP events, the ability to predict different event types using state-of-the-art forecasting systems is still under investigation. For example, the ability of the Australian Bureau of Meteorology coupled ocean-atmosphere seasonal forecast model to predict differences in the SSTA patterns of EP and CP events is limited to less than one season lead time (Hendon et al., 2009). Similarly, Ren et al. (2019) showed that in six operational models the differences in SSTA, precipitation, and teleconnections associated with the two ENSO types could be detected only up to one-month lead time, and only in two or three models. The North American Multimodel Ensemble (Kirtman et al., 2014), which produces ensemble forecasts from a suite of different climate models, shows some skill in capturing the SST and precipitation contrast between central and eastern Pacific warming. However, the models tend to systematically produce more warming in the east, so that strong EP events tend to be better predicted than CP events. Thus, model biases may be responsible for the limited skill in predicting ENSO diversity.

Model studies have also shown that ENSO's seasonal predictability, and seasonal sensitivity to transient external forcings, can depend on the initial flavor of ENSO. In studies with the GFDL-CM2.1 model, Karamperidou et al. (2014) found that active, EP-dominated epochs tended to show greater seasonal predictability than quieter, CP-dominated epochs. In other studies with the CM2.1 model, Predybaylo et al. (2017) showed that the ENSO evolution was most sensitive to tropical explosive volcanic eruptions at the onset of a CP event, with less sensitivity during neutral conditions or at EP event onset, and almost no sensitivity at La Niña onsets.

4.5. LOW-FREQUENCY VARIATIONS OF ENSO DIVERSITY AND CLIMATE CHANGE

The increased intensity and frequency of CP El Niño events since the late 1990s relative to previous decades (Lee & McPhaden, 2010), has suggested the possibility that such changes in ENSO character could be due to global warming. In particular, the 2015–2016 warming of the Niño-4 region, which was extreme by historical standards (L'Heureux et al., 2017), may have included a west Pacific warming trend attributable to anthropogenic forcing (Knutson et al., 2014). It is unclear from the limited observational record, however, whether or not the ENSO SST variability *relative to* this long-term warming trend has changed (Newman et al., 2018). Seasonally resolved coral records spanning the last four centuries indicate that the increased ratio of CP vs. EP events since the late 20th century seemed unusual in the context of that multicentury record, suggesting possible anthropogenic influences on the dominance of CP events in recent decades (Freund et al., 2019).

To help address this question, it is helpful to turn to model simulations. An examination of the Climate Model Intercomparison Project phase 3 (CMIP3) multimodel ensemble showed that the CP vs. EP ratio of occurrence increased in global warming scenario simulations relative to historical simulations (Yeh et al., 2009). In the CMIP5 models, however, results have been more nuanced. Chen et al. (2017) found little consensus among the CMIP5 models regarding the relative likelihood of CP vs. EP events: comparing RCP8.5 projections against preindustrial simulations, roughly as many models showed increases in the likelihood ratio as decreases, and nearly all of those changes were statistically insignificant relative to the unforced variability in the preindustrial control runs. However, like Santoso et al. (2013), Chen et al. (2017) found a robust and statistically significant shift under RCP8.5 forcing toward more eastward propagation of equatorial SSTAs (i.e. a seasonal evolution of individual events from a CP- toward an EP-type SSTA pattern), especially in the more realistic models that had less of a bias toward excessive eastward SSTA propagation in their historical simulations.

Kim and Yu (2012) found that the *intensity* of both CP and EP events strengthened from preindustrial simulations to historical simulations, whereas for RCP4.5 projections the CP events continued to strengthen while the EP events weakened; thus, in the RCP4.5 scenario the CP events became progressively stronger relative to the EP events. This increase in CP intensity relative to EP was attributed to the future changes in the upper ocean thermal stratification in the scenario simulations. Climate models project a weakening of the Walker circulation with global warming (Vecchi et al., 2006a) resulting in a weakened eastern Pacific cold tongue and reduced zonal thermocline slope. These mean state changes are expected to reduce upwelling, thus weakening the thermocline feedback in the eastern Pacific, while the increased stratification of the sloping thermocline in the central Pacific can enhance both the zonal advective feedback (DiNezio et al., 2012) and the thermocline feedback (Dewitte et al., 2013), resulting in a preferred central Pacific warming. On the other hand, Cai et al. (2018) found increased variance in the E index and more frequent strong eastern Pacific El Niño events with climate change in models that represent the nonlinearity in the Bjerknes feedback. This change is associated with the increased stratification of the equatorial Pacific, which enhances the projection of the anomalous wind forcing onto the dominant oceanic baroclinic modes, hence increasing the ocean-atmosphere coupling.

In contrast with the mechanisms proposed in some of the above studies, the CP-dominated 2000–2014 period was characterized by a steeper zonal thermocline slope (McPhaden et al., 2011). This is in agreement with results from single-forcing ensemble simulations of the last millennium, which showed that the relative incidence of CP vs. EP events during the 20th century (1850–2005) compared to the preindustrial period (850–1849) significantly increased in the presence of ozone/aerosol forcing, which is conducive to a stronger zonal tilt of the thermocline. The CP/EP frequency showed no significant change when only greenhouse gas forcing, which produces a reduced zonal thermocline slope, was prescribed (Stevenson et al. 2019). These results not only highlight the complexity of the climate change–ENSO relationship but also support the link between a zonally steeper equatorial thermocline and a higher frequency of CP events. Although most climate models project a weakening of the Walker circulation and a warming of the eastern Pacific cold tongue, other studies based on observations (Compo & Sardeshmukh, 2010; Solomon & Newman, 2012; L'Heureux et al., 2013, Li et al., 2017) suggest an intensification of the equatorial easterly winds and a strengthening of the cold tongue over the 20th century. In particular, Li and colleagues (2017) related the increased frequency of CP El Niño events in recent decades to what they call the cold tongue mode (CTM), a cooling trend of the equatorial cold tongue that emerges as the second EOF of SSTAs based on the HadISST1 dataset over the period 1871–2010, which they attributed to global warming. The colder conditions in the eastern equatorial Pacific associated with the CTM would cause a westward displacement of the ENSO-related air-sea interactions and a weakening of the Bjerknes feedback, resulting in a preferred occurrence of CP-type events (Xiang et al., 2013). Whether the cold tongue is warming or cooling with climate change, and whether these changes in the tropical Pacific climate will influence (or are already influencing) ENSO diversity, remain open questions.

The relative frequency of CP and EP events also appears to undergo natural decadal variations. Newman et al. (2016), for example, show that CP events are more common during the negative phases of the Pacific Decadal Oscillation (PDO), which are (again) associated with stronger trade winds in the tropics and cooler conditions in the eastern equatorial Pacific. EP events, on the other hand, tend to preferentially occur during positive PDO phases. For example, the decade of prevailing CP events at the beginning of the 21st century examined by McPhaden et al. (2011) coincides with a negative phase of the PDO. Influences from other ocean basins could also contribute to the decadal modulation of ENSO diversity. For example, Yu et al. (2015) attributed the intensification of the PMM and the increased frequency of CP El Niño events in recent decades to a phase change of the Atlantic Multidecadal Oscillation (AMO) after the 1990s. The influence of the AMO occurred through a strengthening of the North Pacific Subtropical High and an intensification of the background trade winds, which led to a stronger wind-evaporation-SST feedback and stronger atmosphere-ocean coupling in the subtropical north Pacific. The warm conditions in the tropical North Atlantic associated with the warm phase of the AMO in recent decades have also been invoked as a possible contributor to stronger eastern Pacific cross-equatorial southerly winds, which could have induced a La Niña–like background state in the equatorial Pacific that favored CP events (Hu & Fedorov, 2018). Multicentury preindustrial climate model simulations also show a low-frequency modulation of the CP/EP frequency ratio, with CP-dominated epochs characterized by steeper zonal gradients of SST and thermocline depth relative to EP-dominated decadal epochs (Kug et al., 2010; Choi et al., 2011; Choi et al., 2012; Ogata et al., 2013; Atwood et al., 2017). Perfect-model reforecast experiments with a coupled GCM suggest that this intrinsic component of the low-frequency modulation of ENSO diversity may be fundamentally unpredictable on decadal scales (Wittenberg et al., 2014). Other studies report statistically significant differences in the linear dynamics of observed decadal epochs with different ENSO characteristics (Capotondi & Sardeshmukh, 2017). Such changes in linear dynamics could be consistent with either internal stochastic modulations of stationary but *nonlinear* ENSO dynamics, and/or with a role for external forcings (anthropogenic or natural radiative forcings, or decadal interactions of the tropical Pacific with the extratropics or other tropical basins) in modulating ENSO via changes in the background climate of the tropical Pacific. These results open the question of whether ENSO's observed past behavior has responded in a deterministic fashion to changes in the background conditions, or whether decadal changes in ENSO characteristics have arisen mostly by chance, as seen in unforced climate model simulations (Wittenberg, 2009; Kug et al., 2010; Choi et al., 2011, 2012; Wittenberg et al., 2014).

Changes in background conditions could alter ENSO dynamical feedbacks, and favor either EP or CP events (Luebbecke & McPhaden, 2014). At the same time, changes in ENSO characteristics could rectify into the background state through nonlinearities and temporal blurring of fluctuating climatological features like the ITCZ, cold tongue, and thermocline (Watanabe et al., 2012; Watanabe & Wittenberg 2012; Ogata et al., 2013; Atwood et al., 2017). For example, McPhaden et al. (2011) noticed that changes in composite El Niño SST and thermocline patterns during 2000–2010 (when CP events prevailed) relative to 1980–1999 (when EP events prevailed) resembled the changes in mean SST and thermocline conditions over the two periods, suggesting that the latter may be a rectification of the former. Thus, whether decadal modulation of ENSO diversity is a consequence or a cause of mean state changes remains at this point an important open question that needs to be addressed.

4.6. ENSO DIVERSITY REPRESENTATION IN CLIMATE MODELS

Although the simulation of ENSO in climate models has significantly improved in recent decades, as shown by the large body of literature documenting the CMIP3 and CMIP5 multimodel archives, several aspects of ENSO are still not satisfactorily represented in climate models (Bellenger et al., 2014; see chapter 9 for more details). In particular, many models have difficulty in simulating El Niño events with sufficient diversity in spatial patterns along the equator (Ham & Kug, 2012). This model deficiency is illustrated in Figure 4.7, which compares the composite equatorial profiles of EP and CP El Niño events in observations and in 20 models from the CMIP5 archive. The Niño-3 and Niño-4 indices were used to classify the events. While some models (NCAR-CCSM4, CNRM-CM5, GFDL-CM3, GFDL-ESM2M) show distinct zonal maxima for the two groups of events, somewhat similar to the observations, other models (e.g. HadGEM2-CC, HadGEM2-ES, INM_CM4, MIROC-ESM, MRI-CGCM3) display longitudinal evolutions for the two groups that are strongly overlapping. Chen et al. (2017) found that most of the CMIP5 models tended to produce excessive numbers of CP events relative to EP events.

This limitation in the representation of ENSO diversity likely arises from model biases in the background mean state (Guilyardi et al., 2012a, 2012b; Capotondi et al., 2015b; Guilyardi et al., 2016). In particular, the intensity of the equatorial cold tongue, which helps set the strength of the zonal and meridional SST gradients near the equator, is key for determining how readily atmospheric deep convection spreads into the equatorial eastern Pacific during El Niño. Since anomalous convective activity depends on the total SST relative to the tropical mean SST (He et al., 2018), convective responses to diverse anomalous SST patterns rely on the mean state. If the mean state of the equatorial eastern Pacific is too cold, the eastern Pacific warming will not support local convection, and the atmospheric response will be confined to the west, resulting in a limited range of precipitation and SSTA patterns (Ham & Kug, 2012, Kug et al., 2012). The westward extension of the cold tongue is also important, since it determines the position of the maximum zonal SST gradient. If the cold tongue extends too far west, the ENSO SSTA pattern can take on too much of a "double-peaked" longitudinal structure, in which SSTAs driven by zonal advection in the west are separated from SSTAs driven by vertical advection in the east (Graham et al., 2017).

4.7. CONCLUSIONS

In this chapter we have provided a synthesis of current understanding of ENSO diversity. Our focus has primarily been on El Niño events, since they exhibit a broader range of spatial structures relative to La Niña events (Kug & Ham, 2011). El Niño events vary in amplitude, spatial pattern, and temporal evolution in ways that make each event unique, so that "no two El Niño events are quite alike" (Wyrtki, 1975). Recent studies, using a variety of approaches and criteria, have often partitioned El Niño events into Central Pacific (CP) and Eastern Pacific (EP) types, in order to better represent their dynamics, origin, and evolution. These various approaches have helped identify salient features of the two El Niño groups, including spectral characteristics, temporal evolution, and their outgoing longwave radiation signature as a proxy for event impacts. The decadal variation of CP events, an aspect that has been highlighted in conjunction with some recently proposed indices, is an intriguing phenomenon that needs to be better understood.

Whether EP and CP events are distinct entities or the extreme expressions of a continuum of ENSO flavors remains an open question. On one hand, empirical studies show the emergence of two "modes" resembling the EP and CP cases (Newman et al., 2011), and some degree of bimodality is found when considering extreme El Niño events (Takahashi et al., 2011; Takahashi & Dewitte, 2016; Cai et al., 2018). On the other hand, the broad range of spatial patterns of El Niño events does not seem to support bimodality of equatorial SSTA distributions. Also, both EP and CP events are controlled by the same underlying dynamical processes, although their relative importance is longitudinally dependent. El Niño–related SSTAs in the eastern Pacific are largely controlled by the thermocline feedback, since upwelling is enhanced and vertical temperature gradients are stronger in the eastern Pacific. SSTAs in the central Pacific are more influenced by the zonal advective feedback, due to the larger mean zonal temperature gradients and zonal current variations in that region. Decadal variations in ocean background conditions can perhaps influence the relative frequency of EP and CP events in different decadal epochs, via the spatial modulation of the leading dynamical feedbacks.

Whatever the nature of ENSO diversity, continuous or bimodal, the ability to predict the longitudinal location of the largest equatorial SSTAs is very important for atmospheric teleconnections. Can different event types be skillfully predicted? Different precursors, both within the tropical Pacific as well as from regions outside the tropical Pacific, have been suggested as more conducive to EP or CP events. In particular, the SST and wind anomalies associated with the North Pacific Meridional Mode have been considered as possible triggers of CP El Niño events, while the South Pacific Meridional Mode has been viewed as more conducive to EP El Niño events. However, the initial/background zonal thermocline slope appears to be an important discriminating factor for evolving a developing El Niño into either an EP or CP event. Subsurface ocean conditions with a zonally flatter thermocline are more conducive to the development of EP El Niños, while a zonally steeper thermocline favors CP El Niños. This result emerges from an empirical calculation of the optimal EP and CP precursors and is consistent with results from both observations and long climate model simulations. The processes by which a zonally steeper thermocline favors CP events are still unclear. More importantly, it is still unknown whether these background changes are a cause or a consequence of ENSO diversity, an issue that is in urgent need of clarification. Going forward, continuation of existing long-term observational records in the tropical Pacific

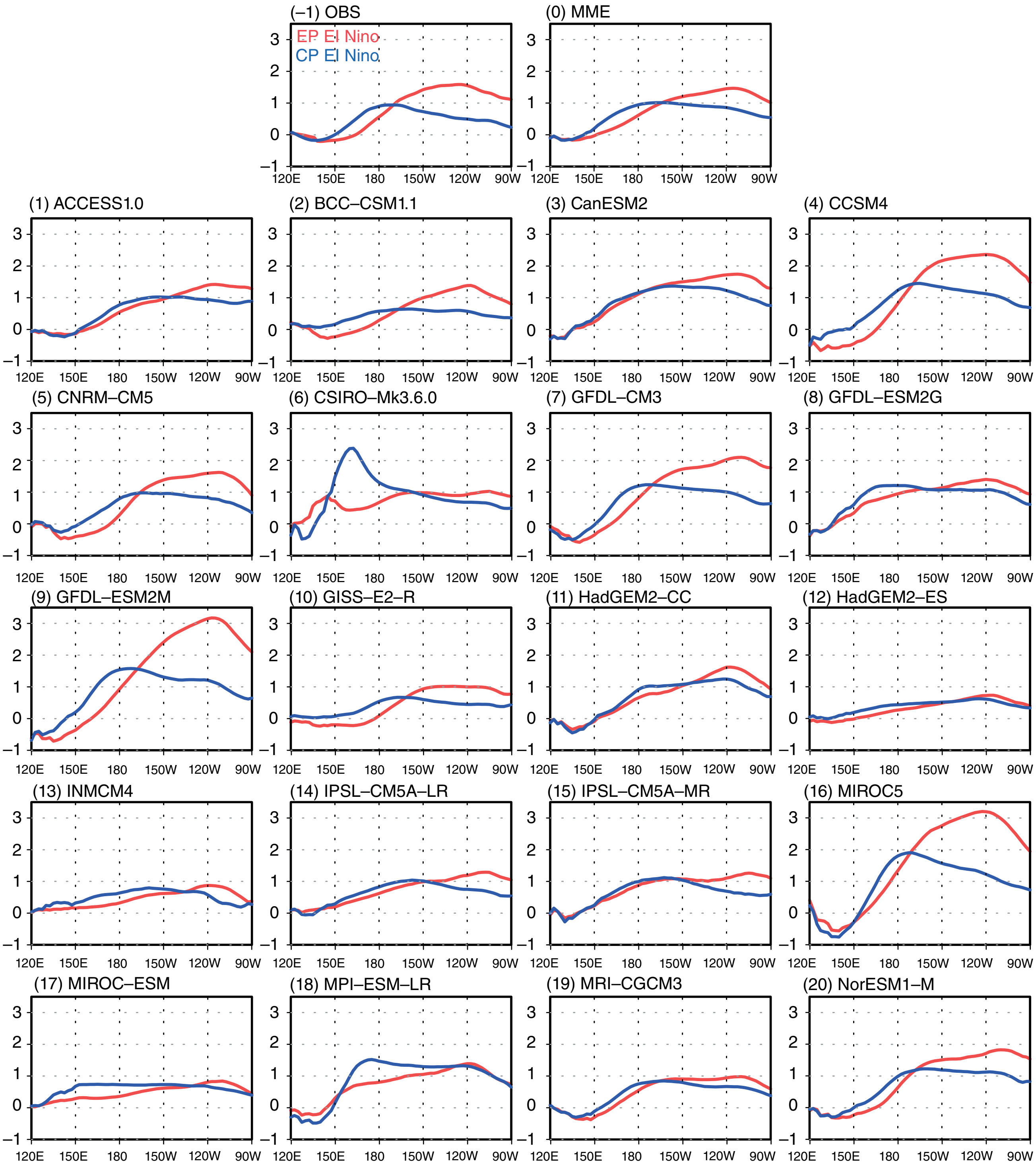

Figure 4.7 Composites of equatorial SSTA profiles averaged in 5°S–5°N for EP (red line) and CP (blue line) events for observations (ERSSTv5; Huang et al., 2017; panel –1) during 1951–2017, the multimodel ensemble mean (panel 0) and 20 models from the CMIP5 archive (panels 1–20). EP and CP events are identified using the normalized Niño-3 and Niño-4 indices, respectively. EP events are characterized by a value of the Niño-3 index greater than one standard deviation, and greater than the value of the Niño-4 index, and vice versa for the CP events. Equatorial profiles are shown as a function of longitude. Vertical axis units are °C (adapted from Capotondi et al., 2015b).

will be needed to understand the full diversity of ENSO events in the real world, together with observational enhancements to underpin future improvements in model simulations (Kessler et al., 2019).

How will ENSO diversity change in a changing climate? The answer to this question depends on the tropical Pacific mean state response to climate change, and on the relationship of ENSO diversity with the underlying background conditions. Whether the equatorial Pacific cold tongue weakens or strengthens with climate change, it is expected to have a large impact on the nature of ENSO and its diverse expressions. Such changes might not be reliably detectable for several decades, however, given the strong intrinsic modulation of ENSO diversity suggested by historical observations and model simulations. Many models still have difficulty simulating ENSO diversity, due in part to the severity of their cold tongue bias. Thus, improved simulation of ENSO diversity by the majority of the next generation of climate models, as well as reliable projections of tropical Pacific mean state climate by those models, are needed to understand how ENSO flavors will change in the future.

APPENDIX: INDICES OF EL NIÑO DIVERSITY

El Niño Modoki index (EMI; Ashok et al., 2007). This index is calculated as EMI = $SST_C - 0.5 * (SST_E + SST_W)$, where SST_C is the average SSTA over the central equatorial Pacific (10°S–10°N, 165°E-140°W), and SST_E and SST_W are SSTA averaged over an eastern (15°S–5°N, 110°–70°W) and a western (10°S–20°N, 125°–145°E) region, respectively. This index was constructed to capture the "Modoki" SSTA pattern, characterized by positive values in the central equatorial Pacific and negative anomalies on the eastern and western sides of the positive anomalies. The original definition by Ashok et al. (2007) also includes the criterion that the anomalous warming in the central Pacific must persist from boreal summer through winter, that is, for three seasons.

Niño-3–Niño-4 approach (Kug et al., 2009; Yeh et al., 2009). This method uses the Niño-3 (average SSTA in 5°S–5°N, 90°–150°W) and Niño-4 (average SSTA in 5°S–5°N, 160°E–150°W) indices to identify cold tongue and warm pool events. Cold tongue events are identified by the criterion that the boreal winter Niño-3 index is larger than one standard deviation (or larger than 0.5°C, depending on the application) and larger than Niño-4, while warm pool events are characterized by the boreal winter Niño-4 index exceeding one standard deviation (or 0.5°C) and exceeding the Niño-3 index.

EP–CP index method (Kao & Yu, 2009; Yu et al., 2012). CP events are defined as the leading empirical orthogonal function (EOF) and associated principal component (PC) of the SSTA after the regression of the SSTA onto the Niño-1+2 index, which is associated with eastern Pacific warming, is removed from the total SSTA field. EP events are obtained as the leading EOF/PC of the SSTA after the regression of the SSTA onto the Niño-4 index, associated with central Pacific warming, is removed from the total SSTA field.

EP–CP subsurface index method (Yu et al., 2011). The EP and CP indices are obtained by averaging the upper 100 m ocean temperature anomalies over the eastern (80°W–90°W, 5°S–5°N) and central (160°E–150°W, 5°S–5°N) equatorial Pacific, respectively, exploiting the fact that CP events have their largest subsurface anomalies in the central Pacific, where EP El Niño events have only weak subsurface anomalies.

N_{CT}–N_{WP} indices (Ren & Jin, 2011). The N_{CT} and N_{WP} indices are obtained as a linear combination of the Niño-3 and Niño-4 indices as: N_{CT} = Niño-3 – αNiño-4, N_{WP} = Niño-4 – αNiño-3, with α = 0.4, when Niño-3 • Niño-4 > 0, and zero otherwise. This approach was motivated by the need of indices for CP and EP El Niño types that were uncorrelated, unlike the Niño-3 and Niño-4 indices.

EP_{new}–CP_{new} indices (Sullivan et al., 2016). These indices are similar to the N_{WP} and N_{CT} indices, respectively, but the Niño-3 and Niño-4 indices are normalized by their standard deviation, and α = 0.5.

TNI index (Trenberth & Stepaniak, 2001). This index is a measure of the SSTA difference between the Niño-1+2 and the Niño-4 regions: TNI = N1+2 – N4, where N1+2 and N4 are the SSTAs averaged over the Niño-1+2 and Niño-4 regions, each normalized by its standard deviation.

E and C indices (Takahashi et al., 2011). The definition of these indices is based on the two leading principal components (PC1 and PC2, respectively) of SSTAs in the 10°S–10°N tropical Pacific band. The C and E indices are defined as $C = (PC1 + PC2)/\sqrt{2}$, and $E = (PC1 - PC2)/\sqrt{2}$, where PC1 > 0 corresponds to positive SSTAs in the eastern equatorial Pacific, and PC2 > 0 corresponds to positive anomalies in the central Pacific and negative anomalies in the far eastern equatorial Pacific. They are independent by construction and identify moderately warm events, primarily in the central equatorial Pacific, and extreme events in the eastern Pacific, respectively.

Sea Surface Salinity (SSS) indices (Singh et al., 2011; Qu & Yu, 2014). The spatial patterns of SSS during EP and CP events, are used to characterize the different El Niño and La Niña types. EP events are characterized by a larger eastward displacement of the eastern edge of the west Pacific fresh pool and of precipitation than are CP events, resulting in different SSS signatures in the two cases. Singh et al. (2011) has used agglomerative hierarchical clustering to determine salinity patterns associated with EP/CP El Niño and EP/CP La Niña events, while Qu and Yu (2014) have shown that SSS variations over a southeastern Pacific region (0°–10°S, 150°–90°W) are well correlated with the El Niño Modoki index.

Indices of spatial shifts in atmospheric convection (Chiodi & Harrison, 2010; Johnson & Kosaka, 2016; Williams & Patricola, 2018). These approaches aim at identifying El Niño events characterized by deep convection in the eastern equatorial Pacific and associated with robust climate impacts over the U.S. Chiodi and Harrison (2010) defined a top-of-atmosphere outgoing longwave radiation (OLR) El Niño index based on the average OLR anomalies over the central Pacific (5°S–5°N, 170°E–100°W). Johnson and Kosaka (2016) identified EPC and EPN (east Pacific convective and nonconvective, respectively) El Niño events based on the value of the relative SST (RSST), defined as the local minus the tropically (20°S–20°N) averaged SST, in an eastern equatorial Pacific box (5°S–5°N, 150°–90°W). RSST values exceeding 0.7 identify EPC events, and RSST values less than 0.7 identify EPN events. Williams and Patricola (2018) define the ENSO Longitude Index (ELI), which identifies the average longitude, within the 5°S–5°N tropical Pacific band, of the points where the local SST is above a convective threshold defined as the SST averaged over the global tropics.

Spatiotemporal indices (Lee et al., 2014). This approach examines interevent variations in both longitude and time, to characterize the diversity among ENSO events of amplitude, spatial pattern, growth, propagation, persistence, decay and transition, and seasonal timing. The first step is to identify a set of events: e.g. El Niño events for which the three-month running mean SSTA averaged over the Niño-3.4 region (5°S–5°N, 120°–170°W) exceeds 0.5 K for at least five consecutive months. For each such event, a longitude-time Hovmöller map of equatorial Pacific SSTAs (averaged 5°S–5°N) is constructed, spanning 120°E–80°W and extending for two years (from January of the onset year to December of the decay year). A PC analysis is then performed on the set of event Hovmöllers. The resulting EOF patterns (which are themselves Hovmöllers) then express the main directions of interevent diversity in spatiotemporal evolution, and the associated PCs express the amount of each EOF present in each particular event.

ACKNOWLEDGMENTS

The authors would like to thank Dr. Y.-G. Ham for his help in preparing one of the figures, and two anonymous reviewers for their excellent and constructive comments. Suggestions received from the participants of an ENSO meeting held in Hobart, Tasmania, 1–2 February 2019 are also gratefully acknowledged. AC was supported by the NASA Physical Oceanography Program (Award NNX15AG46G). This is PMEL contribution no. 4905.

REFERENCES

Anderson, B. T. & R. Perez (2015), ENSO and non-ENSO induced charging and discharging of the equatorial Pacific. *Climate Dynamics*, *45*, 2309-2327.

Ashok, K., S. K. Behera, S. A. Rao, H. Weng, & T. Yamagata (2007). El Niño Modoki and its possible teleconnections. *J. Geophys. Res.*, *112*, C11007. doi:10.1029/2006JC003798

Ashok, K., T. P. Sabin, P. Swapna, & R. G. Murtugudde (2012). Is a global warming signature emerging in the tropical Pacific? *Geophys. Res. Lett.*, *39*, L02701. doi:10.1029/2011GL050232.

Ashok, K., M. Shamal, A. K. Sahai, & P. Swapna (2017). Nonlinearities in the evolutional distinction between El Niño and La Niña types. *J. Geophys. Res. (Oceans)*, *122*, 9649–9662.

Atwood, A. R., D. S. Battisti, A. T. Wittenberg, W. G. H. Roberts, & D. J. Vimont (2017). Characterizing unforced multi-decadal variability of ENSO: A case study with the GFDL CM2.1 coupled GCM. *Climate Dyn.*, *49*(7–8), 2845–2862. doi: 10.1007/s00382-016-3477-9

Balmaseda, M. A., K. Mogensen, & A. T. Weaver (2013). Evaluation of the ECMWF ocean reanalysis system ORAS4. *Q. J. R. Meteorol. Soc.*, *139*, 1132–1161.

Behera, S., & T. Yamagata (2010). Imprint of the El Niño Modoki on decadal sea level changes. *Geophys. Res. Lett.*, *37*, L23702. doi:10.1029/2010GL045936

Bellenger, H., E. Guilyardi, J. Leloup, M. Lengaigne, & J. Vialard (2014). ENSO representation in climate models: from CMIP3 to CMIP5, *Clim. Dyn.*, *42*, 1999–2018.

Brown, J. N., & A.V. Fedorov (2010). How much energy is transferred from the winds to the thermocline on ENSO timescales? *J. Climate*, *23*, 1563–1580.

Cai., W., G. Wang, B. Dewitte, L. Wu, A. Santoso, et al. (2018). Increased variability of eastern Pacific El Niño under greenhouse warming. *Nature*. doi:10.1038/s41586-018-0776-9.

Capotondi, A. (2013). ENSO diversity in the NCAR CCSM4. *J. Geophys. Res.*, *118*, 4755–4770.

Capotondi, A., & P. D. Sardeshmukh (2015). Optimal precursors of different types of ENSO events. *Geophys. Res. Lett.*, *42*, 9952–9960. doi:10.1002/2015GL066171.

Capotondi, A., & P. D. Sardeshmukh (2017). Is El Niño *really* changing?, *Geophys. Res. Lett.*, *44*. doi:10.1002/2017GL074515.

Capotondi, A., et al. (2015a). Understanding ENSO diversity. *Bull. Amer. Meteor. Soc.*, *96*, 921–938. doi:10.1175/BAMS-D-13-00117.1

Capotondi, A., Y.-G. Ham, A. T. Wittenberg, & J.-S. Kug (2015b). Climate model biases and El Niño Southern Oscillation (ENSO) simulation. *US CLIVAR Variations*, *13*(1), 21–25.

Capotondi, A., P.D. Sardeshmukh, & L. Ricciardulli (2018). The nature of the stochastic wind forcing of ENSO. *J. Climate*, *31*, 8081–8099.

Chang, P., L. Zhang, R. Saravanan, D. J. Vimont, J. C. H. Chiang, L. Ji, H. Seidal, & M. K. Tippett (2007). Pacific Meridional mode and El Niño-Southern Oscillation. *Geophys. Res. Lett.*, *34*, L16608. doi:10.1029/2007GL030302

Chen, C., M. A. Cane, A. T. Wittenberg, & D. Chen (2017). ENSO in the CMIP5 simulations: Life cycles, diversity, and responses to climate change. *J. Climate*, *30*(2), 775–801. doi: 10.1175/JCLI-D-15-0901.1

Chen, M., P. Xie, J. E. Janowiak, & P. A. Arkin (2002). Global land precipitation: A 50-year analysis based on gauge observations. *J. Hydrometeorology*, *3*, 249–266.

Chiang, J. C. H., & D. J. Vimont (2004). Analogous Pacific and Atlantic meridional modes of tropical atmosphere ocean variability. *J. Climate*, *17*, 4143–4158.

Chiodi, A. M., & D. E. Harrison (2010). Characterizing warm-ENSO variability in the equatorial Pacific: An OLR perspective. *J. Climate*, *23*, 2428–2439.

Chiodi, A. M., D. E. Harrison, & G. A. Vecchi (2014). Subseasonal atmospheric variability and El Niño waveguide warming: Observed effects of the Madden–Julian oscillation and westerly wind events. *Journal of Climate*, *27*(10), 3619–3642.

Choi, J., S.-I. An, J.-S. Kug, & S.-W. Yeh (2011). The role of mean state on changes in El Niño flavor, *Clim. Dyn.*, *37*, 1205–1215.

Choi, J., S.-I. An, & S.-W. Yeh (2012). Decadal amplitude modulation of two types of ENSO and its relationship with the mean state, *Clim. Dyn.*, *28*, 2631–2644.

Compo, G., & P. D. Sardeshmukh (2010). Removing ENSO-related variations from the climate record, *J. Climate*, *23*, 1957–1978.

Dewitte, B., & K. Takahashi (2019). Diversity of moderate El Niño events evolution: Role of air-sea interactions in the eastern tropical Pacific. *Clim. Dyn.*, *52*, 7455. doi: 10.1007/s00382-017-4051-9

Dewitte, B., S.-W. Yeh, & S. Thual (2013). Reinterpreting the thermocline feedback in the western-central equatorial Pacific and its relationship with the ENSO modulation. *Clim. Dyn.*, *41*, 819–830.

Diamond, M. S., & R. Bennartz (2015). Occurrence and trends of eastern and central Pacific El Niño in different reconstructed SST data sets. *Geophys. Res. Lett.*, *42*, 10,375–10,381. doi: 10.1002/2015GL066469.

DiNezio, P. N., B. P. Kirtman, A. C. Clement, S.-K. Lee, G. A. Vecchi, & A. Wittenberg (2012). Mean climate controls on the simulated response of ENSO to increasing greenhouse gases. *J. Climate*, *25*, 7399–7420. doi: 10.1175/JCLI-D-11-00494.1

Fedorov, A. V., S. Hu, M. Lengaigne, & E. Guilyardi (2015). The impact of westerly wind bursts and ocean initial state on the development, and diversity of El Niño events. *Clim. Dyn.*, *44*, 1381–1401.

Fraser, B. (2017). Peru's floods teach tough lessons, *Nature*, *544*, 405–406.

Freund, M. B., B. J. Henley, D. J. Karoly, HMcGregor, N. J. Abram, & D. Dommenget (2019). *Nature Geoscience*, *12*, 450–455.

Garreaud, R. D. (2018). A plausible atmospheric trigger for the 2017 coastal El Niño, *International Journal of Climatology*, *38*, e1296–31302. doi: 10.1002/joc.5426

Gebbie, G., I. Eisenman, A. Wittenberg, & E. Tziperman (2007). Modulation of westerly wind bursts by sea surface temperature: A semistochastic feedback for ENSO. *J. Atmos. Sci.*, *64*, 3281–3295. doi: 10.1175/JAS4029.1

Giese, B. S., & S. Ray (2011). El Niño variability in simple ocean data assimilation (SODA) 1871–2008. *J. Geophys. Res.*, *116*, C02024. doi: 10.1029/2010JC006695

Goddard, L., & S. G. Philander (2000). The energetics of El Niño and La Niña. *J. Climate*, *13*, 1496–1516.

Graham, F. S., A. T. Wittenberg, J. N. Brown, S. J. Marsland, & N. J. Holbrook (2017). Understanding the double peaked El Niño in coupled GCMs, *Climate Dyn.*, *48*(5), 2045–2063. doi: 10.1007/s00382-016-3189-1

Graham, N. E., & Barnett, T. P. (1987). Sea surface temperature, surface wind divergence, and convection over tropical oceans. *Science*, *238*(4827), 657–659.

Guilyardi, E., et al. (2012a). A first look at ENSO in CMIP5. *CLIVAR Exchanges*, *17*, 29–32.

Guilyardi, E., W. Cai, M. Collins, A. Fedorov, F.-F. Jin, A. Kumar, D.-Z. Sun, & A. Wittenberg (2012b). New strategies for evaluating ENSO processes in climate models. *Bull. Amer. Met. Soc.*, *93*, 235–238. doi: 10.1175/BAMS-D-11-00106.1

Guilyardi, E., A. Wittenberg, M. Balmaseda, W. Cai, M. Collins, M. J. McPhaden, M. Watanabe, & S.-W. Yeh (2016). Fourth CLIVAR workshop on the evaluation of ENSO processes in climate models: ENSO in a changing climate. *Bull. Amer. Meteor. Soc.*, *97*(5), 817–820. doi: 10.1175/BAMS-D-15-00287.1

Ham, Y.-G., & J.-S. Kug (2012). How well do current climate models simulate two types of El Niño? *Clim. Dyn.*, *39*, 383–398.

Ham, Y.-G., J.-S. Kug, & F.-F. Jin (2013a). Sea surface temperature in the north tropical Atlantic as a trigger for El Niño/Southern Oscillation events. *Nature Geoscience*, *6*, 112.

Ham, Y.-G., J.-S. Kug, D. Kim, Y. H. Kim, & D.H. Kim (2013b). What controls phase-locking of ENSO to boreal winter in coupled GCMs? *Clim. Dyn.*, *40*, 1551–1568.

Harrison, D. E., & A. M. Chiodi (2009). Pre and post 1997/1998 westerly wind events and equatorial Pacific cold tongue warming. *J. Climate*, *22*, 568–581.

He, J., N. C. Johnson, G. A. Vecchi, B. Kirtman, A. T. Wittenberg, & S. Sturm (2018). Precipitation sensitivity to local variations in tropical sea surface temperature. *J. Climate*, *31*(22), 9225–9238. doi: 10.1175/JCLI-D-18-0262.1

Hendon, H. H., M. C. Wheeler, & C. Zhang (2007). Seasonal dependence of the MJO-ENSO relationship. *Journal of Climate*, *20(3)*, 531–543.

Hendon, H. H., E. Lim, G. Wang, O. Alves, & D. Hudson (2009). Prospects for predicting two flavors of El Niño. *Geophys. Res. Lett.*, *36*, L19713. doi: 10.1029/2009GL040100.

Hu, S., & A. V. Fedorov (2018). Cross-equatorial winds control El Niño diversity and change. *Nature Climate Change*, *8*, 798–802.

Hu, S., A. V. Fedorov, M. Lengaigne, & E. Guilyardi (2014). The impact of westerly wind bursts on the diversity and predictability of El Niño events: An ocean energetics perspective. *Geophys. Res. Lett.*, *41*, 4654–4663.

Hu, Z.-Z., B. Huang, J. Zhu, A. Kumar, & M. McPhaden (2019). On the variety of coastal El Niño events. *Clim. Dyn.*, *52*, 7537–7552. doi: 10.1007/s00382-018-4290-4

Huang, B., P. W. Thorbe, V. F. Banzon, T. Boyer, G. Chepurin, et al. (2017). Extended Reconstructed Sea Surface Temperature, version 5 (ERSSTv5): Upgrades, validations, and intercomparisons, *J. Climate*, *30*, 8179–8205.

Jadhav, J., S. Panickal, S. Marathe, & K. Ashok (2015). On the possible cause of distinct El Niño types in the recent decades. *Sci. Reports*, *5*, 17009. doi: 10.1038/srep17009

Jin, F.-F. (1997). An equatorial ocean recharge paradigm for ENSO. *Part I: Conceptual model. J. Atmos. Sci.*, *54*, 811–829.

Johnson, N. C., & Y. Kosaka (2016). The impact of eastern equatorial Pacific convection on the diversity of boreal winter El Niño teleconnection patterns. *Clim. Dyn.*, *47*, 3737–3765.

Kalney, E., et al. (1996). The NCEP/NCAR 40-year reanalysis project. *Bull. Amer. Meteor. Soc.*, *77*, 437–471.

Kao, H.-Y. & J.-Y. Yu (2009). Contrasting eastern-Pacific and eentral-Pacific types of ENSO. *Journal of Climate*, *22*, 615–632. doi: 10.1175/2008JCLI2309.1

Karamperidou, C., M. A. Cane, U. Lall, & A. T. Wittenberg (2014). Intrinsic modulation of ENSO predictability viewed through a local Lyapunov lens. *Climate Dyn.*, *42*, 253–270. doi: 10.1007/s00382-013-1759-z

Kessler, W. S., et al. (2019). Second report of TPOS 2020. GOOS-234, 265 pp. Available online at http://tpos2020.org/project-reports/second-report and https://doi.org/10.13140/RG.2.2.17161.29289

Kim, S. T., & J.-Y. Yu (2012). The two types of ENSO in CMIP5 models. *Geophys. Res. Lett.*, *39*, L11704. doi: 10.1029/2012GL052006.

Kirtman, B. P., et al. (2014). The North American multimodel ensemble. *Bull. Amer. Meteor. Soc.*, *95*, 585–601. doi: 10.1175/BAMS-D-12-00050.1

Knutson, T. R., F. Zeng, & A. T. Wittenberg (2014). Multimodel assessment of extreme annual-mean warm anomalies during 2013 over regions of Australia and the western tropical Pacific. Section 8 of "Explaining extreme events of 2013 from a climate perspective." *Bull. Amer. Meteor. Soc.*, *95* (9), S26–S30. doi: 10.1175/1520-0477-95.9.S1.1

Kug, J.-S., & Y.-G. Ham (2011). Are there two types of La Niña? *Geophys. Res. Lett.*, *38*. doi:10.1029/2011GL048237.

Kug, J.-S., F.-F. Jin, K.P. Sooraj, & I.-S. Kang (2008). State-dependent atmospheric noise associated with ENSO. *Geophys. Res. Lett.*, *35*, L05701. https://doi.org/10.1029/2007GL032017

Kug, J.-S., F.-F. Jin, & S.-I. An (2009). Two types of El Niño: Cold tongue El Niño and warm pool El Niño. *J. Climate*, *22*, 1499–1515.

Kug, J.-S., et al. (2010). Warm pool and cold tongue El Niño events as simulated by the GFDL CM2.1 coupled GCM. *J. Climate*, *23*, 1226–1239. doi: 10.1175/2009JCLI3293.1

Kug, J.-S., Y.-G. Ham, J.-Y. Lee, & F.-F. Jin (2012). Improved simulation of two types of El Niño in CMIP5 models. *Environ. Res. Lett.*, *7*. doi: 10.1088/1748-9326/3/034002

Larkin, N. K., & D. E. Harrison (2005). On the definition of El Niño and associated seasonal average U.S. weather anomalies. *Geophys. Res. Lett.*, *32* L13705. doi: 10.1029/2005GL022738

Lee, S.-K., P. Di Nezio, E.-S. Chung, S.-W. Yeh, A. T. Wittenberg, & C. Wang (2014). Spring persistence, transition, and resurgence of El Niño. *Geophys. Res. Lett.*, *41*, 8578–8585. doi:10.1002/2014GL062484

Lee, S.-K., A. T. Wittenberg, D. B. Enfield, S. J. Weaver, C. Wang, & R. M. Atlas (2016). U.S. regional tornado outbreaks and their links to spring ENSO phases and North Atlantic SST variability. *Environ. Res. Lett.*, *11*(4), 044008. doi: 10.1088/1748-9326/11/4/044008

Lee, S.-K., H. Lopez, E.-S. Chung, P. DiNezio, S.-W. Yeh, & A. T. Wittenberg (2018). On the fragile relationship between El Niño and California rainfall. *Geophys. Res. Lett.*, *45*(2), 907–915. doi: 10.1002/2017GL076197

Lee, T., & M. J. McPhaden (2010). Increasing intensity of El Niño in the central-equatorial Pacific. *Geophys. Res. Lett.*, *37*, L14603. doi: 10.1029/2010GL044007

Lengaigne, M., E. Guilyardi, J. P. Boulanger, C. Menkes, P. Delecluse, P. Inness, J. Cole, & J. Slingo (2004). Triggering of El Niño by westerly wind events in a coupled general circulation model. *Clim. Dyn.*, *23*, 601–620.

L'Heureux, M., S. Lee, & B. Lyon (2013). Recent multidecadal strengthening of the Walker circulation across the tropical Pacific. *Nat. Climate Change*, *3*, 571–576.

L'Heureux, M. L., K. Takahashi, A. B. Watkins, et al. (2017) Observing and predicting the 2015/16 El Niño. *Bull. Amer. Meteor. Soc.*, *98*(7), 1363–1382. doi: 10.1175/BAMS-D-16-0009.1

Levine, A. F. Z., F.-F. Jin, & M. J. McPhaden (2016). Extreme noise–extreme El Niño: How state-dependent noise forcing creates El Niño-La Niña asymmetry. *J. Climate*, *29*, 5483–5499. doi: http://dx.doi.org/10.1175/JCLI-D-16-0091.1.

Li, Y., J. Li, W. Zhang, Q. Chen, J. Feng, F. Zheng, et al. (2017). Impacts of the tropical Pacific cold tongue mode on ENSO diversity under global warming. *J. Geophys. Res. (Oceans)*, *122*, 8524–8542.

Linkin, M. E., & S. Nigam (2008). The North Pacific oscillation–West Pacific teleconnection pattern: Mature-phase structure and winter impacts. *J. Climate*, *21*, 1979–1997.

Lopez, H., & Kirtman, B. P. (2014). WWBs, ENSO predictability, the spring barrier and extreme events. *J. Geophys. Res.*, *119*, 10,114–10,138. doi: 10.1002/2014JD021908

Luebbecke, J. F., & M. J. McPhaden (2014). Assessing the 21st century shift in ENSO variability in terms of the Bjerknes stability index, *J. Climate*, *27*, 2577–2587. http://dx.doi.org/10.1175/JCLI-D-13-00438.1

Marathe, S., K. Ashok, P. Swapna, & T. P. Sabin (2015). Revisiting El Niño Modokis. *Clim. Dyn.*, *45*, 3527–3545.

McPhaden, M. J. (1999). Genesis and evolution of the 1997-98 El Niño. *Science*, *283*, 950–954.

McPhaden, M. J. (2004). Evolution of the 2002-03 El Niño. *Bull. Amer. Meteor. Soc.*, *85*, 677–695. doi: 10.1175/BAMS-85-5-677

McPhaden, M. J. (2012). A 21st century shift in the relationship between ENSO SST and warm water volume anomalies. *Geophys. Res. Lett.*, *39*, L09706. doi: 10.1029/2012GL051826

McPhaden, M. J., & X. Zhang (2009). Asymmetry in zonal phase propagation of ENSO sea surface temperature anomalies. *Geophys. Res. Lett.*, *36*, L13703. doi: 10.1029/2009GL038774

McPhaden, M. J., X. Zhang, H. H. Hendon, & M. C. Wheeler (2006). Large scale dynamics and MJO forcing of ENSO variability. *Geophysical Research Letters*, *33*(16), L16702. doi: 10.1029/2006GL026786

McPhaden, M. J., T. Lee, & D. McClurg (2011). El Niño and its relationship to changing background conditions in the tropical Pacific. *Geophys. Res. Lett.*, *38*, L15709. doi: 10.1029/2011GL048275

Meinen, C. S., & M. J. McPhaden (2000). Observations of warm water volume changes in the equatorial Pacific and their relationship to El Niño and La Niña. *Journal of Climate*, *13*, 3551–3559.

Newman, M., S.-I. Shin, & M. A. Alexander (2011). Natural variations in ENSO flavors. *Geophys. Res. Lett.*, *38*, L14705. https://doi.org/10.1029/2011GL047658

Newman, M., et al. (2016). The Pacific decadal oscillation, revisited, *J. Climate*, *29*, 4399–4427. doi: 10.1175/JCLI-D-15-0508.1

Newman, M., A. T. Wittenberg, L. Cheng, G. P. Compo, & C. A. Smith (2018). The extreme 2015/16 El Niño, in the context of historical climate variability and change, Section 4 of "Explaining extreme events of 2016 from a climate perspective." *Bull. Amer. Meteor. Soc.*, *99*(1), S16–S20. doi: 10.1175/BAMS-D-17-0116.1

Ogata, T., S.-P. Xie, A. Wittenberg, & D.-Z. Sun (2013). Interdecadal amplitude modulation of El Niño/Southern Oscillation and its impacts on tropical Pacific decadal variability. *J. Climate*, *26*, 7280–7297. doi: 10.1175/JCLI-D-12-00415.1

Paek, H., J.-Y. Yu, & C. Qian (2017). Why were the 2015/2016 and 1997/1998 extreme El Niño different? *Geophys. Res. Lett.*, *44*, 1848–1856.

Peng, Q., Xie, S. P., Wang, D., Zheng, X. T., & Zhang, H. (2019), Coupled ocean-atmosphere dynamics of the 2017 extreme coastal El Niño. *Nature Communications*, *10*(1), 1–10. doi: 10.1038/s41467-018-08258-8

Penland, C., & P. D. Sardeshmukh (1995). The optimal growth of tropical sea surface temperature anomalies. *J. Climate*, *8*, 1999–2024.

Predybaylo, E., G. Stenchikov, A. T. Wittenberg, & F. Zeng (2017). Impacts of a Pinatubo-scale volcanic eruption on ENSO. *J. Geophys. Res. Atmos.*, *122*, 925–947. doi: 10.1002/2016JD025796

Puy, M., J. Vialard, M. Lengaigne, & E. Guilyardi (2016). Modulation of equatorial Pacific westerly/easterly wind events by the Madden-Julian oscillation and convectively-coupled Rossby waves. *Clim. Dyn.*, *46*(7), 2155–2178. doi:10.1077/s00382-015-2695-x

Puy, M., J. Vialard, M. Lengaigne, E. Guilyardi, P. Di Nezio, A. Voldoire, et al. (2019). Influence of westerly wind events stochasticity on El Niño amplitude: The case of 2014 vs. 2015. *Clim. Dyn.*, *52*, 7435–7454. doi: 10.1007/s00382-017-3938-9

Qu, T., & J.-Y. Yu (2014). ENSO indices from sea surface salinity observed by Aquarius and Argo. *Journal of Oceanography*, *70*, 367–375.

Rasmusson, E. M., & T. H. Carpenter (1982). Variations in tropical sea surface temperature and surface wind fields associated with the Southern Oscillation/El Niño. *Mon. Wea. Rev.*, *110*, 354–384.

Ren, H.-L., & F.-F. Jin (2011). Niño indices for two types of ENSO, *Geophys. Res. Lett.*, *38*. doi: 10.1029/2010GL046031.

Ren, H. L., A. A. Scaife, N. Dunstone, B. Tian, Y. Liu, S. Ineson, et al. (2019). Seasonal predictability of winter ENSO types in operational dynamical model predictions. *Climate Dynamics*, *52*(7-8), 3869–3890. doi: 10.1007/s00382-018-4366-1

Reynolds, R. W., N. A. Rayner, T. M. Smith, D. C. Stokes, & W. Wang (2002). An improved in situ and satellite SST analysis for climate, *J. Climate*, *15*, 1609–1625.

Rogers, J. C. (1981). The North Pacific Oscillation, *Int. J. Climatol.*, *1*, 39–57.

Santoso, A., S. McGregor, F.-F. Jin, W. Cai, M. H. England, S.-I. An, et al. (2013). Late 20th century emergence of El Niño propagation asymmetry and future projections. *Nature*, *504*, 126–130.

Santoso, A., M. McPhaden, & W. Cai (2017). The defining characteristics of ENSO extremes and the strong 2015/2016 El Niño. *Rev. Geophys.*, *55*. doi: 10.1002/2017RG000560

Schott, G. (1931). Der Peru-Strom und seine nördlichen Nachbargebiete in normaler und anormaler Ausbildung. *Ann Hydrogr Mar Meteor*, *59*, 161–169, 200–213, 240–257.

Singh, A., T. Delcroix, & S. Cravatte (2011). Contrasting the flavors of El Niño-Southern Oscillation using sea surface salinity observations, *J. Geophys. Res.*, *116*. doi: 10.1029/2010JC006862

Solomon, A., & M. Newman (2012). Reconciling disparate twentieth-century Indo-Pacific ocean temperature trends in the instrumental record. *Nat. Climate Change*, *2*, 691–699.

Stevenson, S., A. Capotondi, J. Fasullo, B. Otto-Bliesner (2019),2017). Forced changes to twentieth century ENSO diversity in a last millennium context, *Clim. Dyn.*, *52*, 7359–7374. doi: 10.1007/s00382-017-3573-5

Sullivan, A., J.-J. Luo, A. C. Hirst, D. Bi, W. Cai, & J. He (2016). Robust contribution of decadal anomalies to the frequency of central Pacific El Niño. *Sci. Rep.*, *6*, 38540. doi: 10.1038/srep38540

Takahashi, K., & B. Dewitte (2016). Strong and moderate nonlinear ENSO regimes. *Climate Dynamics*, *46*, 1627–1645.

Takahashi, K., & A. G. Martinez (2019). The very strong coastal El Niño in 1925 in the far-eastern Pacific. *Clim. Dyn.*, *52*, 7389–7415. doi: 10.1007/s00382-017-3702-1

Takahashi, K., A. Montecinos, K. Goubanova, & B. Dewitte (2011). ENSO regimes: Reinterpreting the canonical and Modoki El Niño.

Takahashi, K., C. Karamperidou, & B. Dewitte (2019). A theoretical model of strong and moderate El Niño regimes. *Climate Dynamics*, *52*, 7477–7493. doi: 10.1007/s00382-018-4100-z.

Takahashi, K., V. Aliaga-Nestares, G. Avalos, M. Bouchon, A. Castro, L. Cruzado, et al. (2018). The 2017 coastal El Niño. In "State of the Climate in 2017." *Bulletin of the American Meteorological Society*, *99*(8), S210–S211.

Timmermann, A., S.-I. An, J.-S. Kug, F.-F. Jin, W. Cai, et al. (2018). El Niño Southern Oscillation complexity. *Nature*, *559*, 535–545. doi: 10.1038/s41586-018-0252-6

Trenberth, K. E., & D. P. Stepaniak (2001). Indices of El Niño evolution. *J. Climate*, *14*, 1697–1701.

Vecchi, G. A., B. J. Soden, A. T. Wittenberg, I. M. Held, A. Leetma, & M. J. Harrison (2006a). Weakening of tropical Pacific atmospheric circulation due to anthropogenic forcing. *Nature*, *441*, 73–76. doi: 10.1038/nature04744

Vecchi, G. A., A. T. Wittenberg, & A. Rosati (2006b). Reassessing the role of stochastic forcing in the 1997–8 El Niño. *Geophys. Res. Lett.*, *33*, L01706. doi: 10.1029/2005GL024738

Vimont, D. J., M. A. Alexander, & M. Newman (2014). Optimal growth of central and east Pacific ENSO events, *Geophys. Res. Lett.*, *41*. doi: 10.1002/2014GL059997

Wang, S.-Y., M. L'Heureux, & H.-H. Chia (2012). ENSO prediction one year in advance using western North Pacific sea surface temperatures. *Geophys. Res. Lett.*, *39*, L05702. doi: 10.1029/2012GL050909

Watanabe, M., & A. T. Wittenberg (2012). A method for disentangling El Niño-mean state interaction. *Geophys. Res. Lett.*, *39*, L14702. doi: 10.1029/2012GL052013

Watanabe, M., J.-S. Kug, F.-F. Jin, M. Collins, M. Ohba, & A. T. Wittenberg (2012) Uncertainty in the ENSO amplitude change from the past to the future. *Geophys. Res. Lett.*, *39*, L20703. doi: 10.1029/2012GL053305

Williams, I. N., & C. M. Patricola (2018). Diversity of ENSO events unified by convective threshold sea surface temperature: A nonlinear ENSO index, *Geophys. Res. Lett.*, *45*, 9236–9244.

Wittenberg, A. T. (2009). Are historical records sufficient to constrain ENSO simulations? *Geophys. Res. Lett.*, *36*, L12702. doi: 10.1029/2009GL038710

Wittenberg, A. T., A. Rosati, T. L. Delworth, G. A. Vecchi, & F. Zeng (2014). ENSO modulation: Is it decadally predictable? *J. Climate*, *27*, 2667–2681. doi: 10.1175/JCLI-D-13-00577.1

Wyrtki, K. (1975). El Niño: The dynamic response of the equatorial Pacific Ocean to atmospheric forcing. *J. Phys. Oceanogr.*, *5*, 572–594.

Xiang, B., B. Wang, & T. Li (2013). A new paradigm for the predominance of standing central Pacific warming after the late 1990s. *Clim. Dyn.*, *41*, 327–340, doi: 10.1007/s00382-012-1427-8

Xie, S.-P. (1999). A dynamic ocean-atmosphere model of the tropical Atlantic decadal variability. *J. Climate*, *12*, 64–70.

Yeh, S.-W., J.-S. Kug, B. Dewitte, M.-H. Kwon, B. P. Kirtman, & F.-F. Jin (2009). El Niño in a changing climate. *Nature*, *461*. doi: 10.1038/nature08316.

Yu, J.-Y., & S. T. Kim (2011). Relationships between extratropical sea level pressure variations, and the central-Pacific and eastern-Pacific types of ENSO. *J. Climate*, *24*, 708–720.

Yu, J.-Y., H.-Y. Kao, T. Lee, & S.-T. Kim (2011). Subsurface ocean temperature indices for central-Pacific and eastern-Pacific types of El Niño and La Niña events. *Theor. Appl. Climatol.*, *103*, 337–344.

Yu, J.-Y., M.-M. Lu, & S.-T. Kim (2012). A change in the relationship between tropical central Pacific SST variability and the extratropical atmosphere around 1990. *Env. Res. Lett.*, *7*. doi: 10.1088/1748-9326/7/3/034025

Yu, J.-Y., P.-K. Kao, H. Paek, H.-H. Hsu, C.-W. Hung, M.-M. Lu, & S.-I. An (2015). Linking emergence of the central-Pacific El Niño to the Atlantic multi-decadal oscillation. *J. Climate*, *28*, 651–662.

Yu, L., R. A. Weller, & T. W. Liu (2003). Case analysis of a role of ENSO in regulating the generation of westerly wind bursts in the western equatorial Pacific. *J. Geophys. Res*, *108*(C4), 3128. doi: 10.1029/2002JC001498

Zhang, H., A. Clement, & P. Di Nezio (2014). The South Pacific meridional mode: A mechanism for ENSO-like variability. *J. Climate*, *27*, 769–783.